



RAPPORTO TECNICO - TECHNICAL REPORT

METIS INSTRUMENT PROPOSAL

for the Solar Orbiter Mission

Part 1: Scientific and Technical Plan

Ester Antonucci (P.I.), S. Fineschi, G. Naletto, M. Romoli, D. Spadaro, S.
Solanski, P. Lami and the Co-I's Team

Rapporto nr. 93

14/01/2008

**METIS INSTRUMENT PROPOSAL
for the
Solar Orbiter Mission**

Part I

SCIENTIFIC AND TECHNICAL PLAN

Principal Investigator:

Ester Antonucci (1)

Co-Proposers:

**S. Fineschi (1), G. Naletto (2), M. Romoli (3), D. Spadaro (4),
S. Solanki (5), P. Lamy (6), and the Co-I's Team**

- (1) INAF – Astronomical Observatory of Turin, Torino, Italy**
- (2) University of Padua, Padova, Italy**
- (3) University of Florence, Firenze, Italy**
- (4) INAF - Astrophysical Observatory of Catania, Italy**
- (5) Max-Planck-Institute fuer Sonnensystemforschung, Germany**
- (6) Laboratoire d'Astrophysique de Marseille, France,**

Leading Funding Agency:

ASI – Agenzia Spaziale Italiana
(Ref. S. Di Pippo – simonetta.dipippo@asi.it) - Viale Liegi 26 – 00198 Roma Italy
Phone: +390685671 Fax: +39 06 8567267)

In cooperation with:

CNES – Centre National d'Etudes Spatiale
DLR – Detuches Zentrum fuer Luft und Raumfahrt

This proposal can be electronically retrieved at the following address:

http://amenophi.oato.inaf.it/METIS/?page_id=95

Project Contact Directory

Name	Role	Affiliation and Address	Contact informations
Ester Antonucci	PI	INAF Osservatorio Astronomico di Torino Via dell'Osservatorio, 20 10025 Pino Torinese TO, Italy	+39 011 8101913 Office +39 011 8101930 Fax antonucci@oato.inaf.it
Silvano Fineschi	METIS Investigation Scientist / Co-I	INAF Osservatorio Astronomico di Torino Via dell'Osservatorio, 20 10025 Pino Torinese TO, Italy	+39 011 8101919 Office +39 011 8101930 Fax fineschi@oato.inaf.it
Giampiero Naletto	METIS Experiment Manager / Co-I	University of Padova Department of Information Engineering Via Gradenigo, 6/B 35131 Padova PD, Italy	+39 049 8277646 Office +39 049 8277699 Fax naletto@dei.unipd.it
Marco Romoli	Co-PI (COR)	University of Florence Department of Astronomy and Space Science Largo Enrico Fermi, 2 50125 Firenze FI, Italy	+39 055 2307767 Office +39 055 224193 Fax romoli@arcetri.astro.it
Angela Ciaravella	Investigation Scientist (COR – Coronal Imaging) / Co-I	INAF Osservatorio Astronomico di Palermo Piazza del Parlamento, 1 90134 Palermo PA, Italy	+39 091 233454 Office +39 091 233-444 Fax ciarave@astropa.unipa.it
Luca Zangrilli	Instrument Scientist (COR) / Co-I	INAF Osservatorio Astronomico di Torino Via dell'Osservatorio, 20 10025 Pino Torinese TO, Italy	+39 011 8101913 Office +39 011 8101930 Fax zangrilli@oato.inaf.it
Daniele Spadaro	Co-PI (EUS)	INAF Osservatorio Astronomico di Catania Via S. Sofia, 78 95123 Catania CT, Italy	+39 095 7332234 Office +39 095 7330592 Fax dspadaro@oact.inaf.it
Vincenzo Andretta	Investigation Scientist (EUS – Disk Spectroscopy) / Co-I	INAF Osservatorio Astronomico di Capodimonte Salita Moiarriello, 16 8013 Napoli NA, Italy	+39 081 5575524 Office +39 081 5575433 Fax andretta@oacn.inaf.it
Luca Poletto	Instrument Scientist (EUS) / Co-I	CNR-INFM-LUXOR c/o Department of Information Engineering Via Gradenigo 6/B, 35131 Padova PD, Italy	+39 049 8277680 Office +39 049 8277699 Fax poletto@dei.unipd.it
Sami Solanky	Co-I	Max-Planck-Institut fuer Sonnensystemforschung Max-Planck-Str. 2 37191 Katlenburg-Lindau, Germany	+49-5556-979 325 Office +49-5556-979 190 Fax solanky@mps.mpg.de
Philippe Lamy	Co-I	Laboratoire d'Astrophysique de Marseille BP 8 - Traverse du Siphon 13376 Marseille CEDEX 12 France	+33 (04)91055900 Office +33 (04)91661855 Fax philippe.lamy@oamp.fr

Distribution

Name	Organisation
Marcello Coradini	ESA/HQ (D/SCI) 8-10 rue Mario Nikis 75738 Paris Cedex 15 France
Richard Marsden	ESA/ESTEC (SCI-SM) + P.O. Box 299 1 (part VI) 2200 AG Noordwijk The Netherlands
Philippe Kletzkin	ESA/ESTEC (SCI-P) + P.O. Box 299 1 (part VI) 2200 AG Noordwijk The Netherlands
Simonetta Di Pippo	ASI – Osservazione dell'Universo Viale Liegi, 26 00198 Roma, Italia
Prof. Sergio De Julio	INAF Viale del Parco Mellini n.84 00136 Roma

Table of Contents

1	EXECUTIVE SUMMARY	8
1.1	The Science	8
1.2	The innovation.....	9
1.3	The Instrument.....	9
1.4	Instrument Operations and Scientific analysis.....	10
1.5	The Consortium.....	10
1.6	METIS data sheet.....	11
2	SCIENTIFIC OBJECTIVES	13
2.1	METIS Investigation.....	13
2.2	Mapping the origins of the solar wind streams.....	14
2.2.1	The case of the slow wind	14
2.2.1.1	Slow wind sources identified with He abundance measurements	15
2.2.1.2	Role of magnetic topology in controlling the solar wind properties	15
2.2.2	The case of the fast solar wind.....	16
2.2.2.1	Role of the magnetic structure in controlling the solar wind emergence	16
2.2.2.2	Identifying the solar wind sources on the basis of the elemental composition.....	16
2.2.2.3	Determining the role of plumes in the generation of the fast wind	17
2.3	Understanding the plasma heating and acceleration of the solar wind	17
2.3.1	Energy deposition in the fast solar wind via ion cyclotron dissipation of fast Alfvén waves.....	17
2.3.2	Reconnection of closed and open structures as sources of waves and turbulence to heat the fast solar wind.....	18
2.3.3	Which is the origin of turbulence in the solar wind?	18
2.4	Which are the sources of solar energetic particles (SEPs).....	19
2.5	Investigating the evolution of coronal mass ejections in the inner heliosphere	19
2.5.1	Study of the longitudinal structure of the active Sun.....	20
2.5.2	Spectroscopic detection of cool ($\sim 10^4$ K) plasma ejected in the inner heliosphere	20
2.5.3	Spectroscopic detection of plasma heated by reconnection events after the CME front transit	20
2.5.4	Observation of plasma shock heating at the CME front	20
2.6	Determining the nature of the energy deposition and dissipation mechanisms.....	21
2.7	Structure and evolution of streamers	22
2.8	Solar Orbiter Mission Requirements	22
2.8.1	Solar Orbiter spacecraft performance	22
2.8.2	Solar Orbiter orbit.....	22
2.8.3	Other Solar Orbiter payload elements	23
2.8.4	Ground segment.....	23

3	INSTRUMENT PERFORMANCES	23
3.1	COR: Visible light and UV Coronagraphic-Imager	23
3.1.1	Instrument Observational Parameters and Sensitivities	23
3.1.2	Expected Countrates	25
3.2	EUS Extreme UV Spectrometer	26
3.2.1	Instrument Observational Parameters and Sensitivities	27
3.2.2	Expected Countrates	28
3.3	SOCS: Solar Orbiter Coronal Spectrometer	29
3.3.1	SOCS Instrument Observational Parameters and Sensitivities	29
3.3.2	Expected countrates	30
3.4	Summary of the METIS Elements performances	31
4	INSTRUMENT TECHNICAL DESCRIPTION AND DESIGN	34
4.1	Functional description	34
4.1.1	Combined Configuration METIS	34
4.1.2	COR	34
4.1.3	EUS.....	35
4.1.4	SOCS	35
4.2	Hardware description	35
4.2.1	Optical Design	35
4.1.1.1	Design of the coronagraph	35
4.1.1.2	Design of the spectrometer.....	36
4.1.1.3	Design of the spectro-coronagraph	37
4.2.2	Thermo Mechanical Design.....	38
4.2.3	Mechanisms	40
4.2.4	Detectors and Front-End Electronics	40
4.1.1.4	COR detectors	40
4.1.1.5	EUS/SOCS detectors.....	40
4.2.5	Electronics	41
4.3	Software description	43
4.4	Operational modes	43
4.5	Critical Technologies	44
4.1.2	Polarimeter	44
4.1.3	Multilayers for COR and SOCS	44
4.1.4	IAPS Detectors for EUS/SOCS	44
4.6	Minimum METIS configuration	44
5	SUMMARY OF EXPERIMENT INTERFACES	45
5.1	External Configuration Drawings	45
5.2	Summary of METIS interfaces	45
6	TEST AND CALIBRATION PLAN	46

6.1	Testing	46
6.1.1	Ground/pre launch Tests.....	46
6.1.1.1	Sub-system tests.....	46
6.1.1.2	Element tests.....	46
6.1.1.3	Instrument tests.....	46
6.1.1.4	S/C tests.....	46
6.1.2	Cruise Tests.....	46
6.1.3	In orbit Tests.....	47
6.2	Calibration	47
6.2.1	Ground/pre launch Calibrations.....	47
6.2.1.1	Calibration at element level.....	47
6.2.1.2	Calibration at Instrument level.....	48
6.2.1.3	Calibration at System level.....	48
6.2.2	Cruise Calibrations.....	48
6.2.3	In orbit Calibrations.....	48
7	SYSTEM LEVEL AIV	48
7.1	Verification Program	48
7.2	Model Philosophy	49
7.3	System Integration and Test Flow	49
7.4	Ground Support Equipment	50
8	FLIGHT OPERATIONS CONCEPT	50
8.1	Observing concept	50
8.2	In-Flight Calibrations	51
8.3	Support to MOC and SOC	51
9	DATA REDUCTION, SCIENTIFIC ANALYSIS AND ARCHIVAL SUPPORT	52
9.1.1	Pre-launch phase.....	52
9.1.2	Cruise and Operation phase.....	52
9.1.3	Data reduction process.....	52
9.1.4	Scientific data analysis.....	53
9.1.5	Data archiving.....	53
9.2	Compliance with the Agency scientific data policy	53
10	DOCUMENT REFERENCES	54
10.1	Scientific Reverences	54
10.1.1	Chapter 2 – Scientific Objectives.....	54
10.1.2	Chapter 3 - Instrument Performances.....	55
10.1.3	Chapter 4 - Instrument Technical Description and Design.....	55
11	ACRONYMS	57

LIST OF FIGURES

Figure 1: Left: COR field-of-view at 0.22 AU: beginning of mission perihelion (1.2-3 Ro). Right: COR FOV at 0.5 AU (2.7-6.7 Ro). Nominal observations start below this distance	24
Figure 2: COR FOV during S/C offset pointing.	24
Figure 3: Left: Reflectivity of the SiC/Mg EUV multilayer with cap-layer. Right: Effective area in the 3 COR channels.....	25
Figure 4 Count-rates for observations from 0.22 AU, perihelion at the beginning of mission.....	25
Figure 5 Count-rates for observations from 0.3 AU, perihelion at the end of nominal mission.	26
Figure 6: Wavelengths bands accessed by METIS EUS	27
Figure 7: Formation temperatures of the ions whose lines are observed in the EUS channels . Color coding for line temperatures is: red for "chromospheric" lines; orange "transition region", green "coronal" and blue "flare".....	28
Figure 8: Simulated Quiet Sun spectral count rates in Band B. First order spectrum is shown in black; second order spectrum in green. Bare detector areas are shown as grey bands. The shaded band centred at 121.6 nm is the Ly- α attenuator for reducing the intense flux of this line.....	28
Figure 9: The SOCS's multislit defines four instantaneous FOVs at different angular distances from the solar West limb. Left: physical FOV covered by the multislit at 0.22 AU. Right: the same at 0.38 AU. The upper right insets show the full 2-D images reconstructed by interpolating the four simultaneous 1-D images. The lower left insets show disk images obtained from EUS (17-arcmin) ² rasters.	30
Figure 10 Effective areas of the 3 SOCS channels for each of the 4 slits (in the HeII channel only the images of 2 slits fall on the detector C).	30
Figure 11: SOCS OVI detector simulated composite spectrum at 0.3 AU	30
Figure 12: SOCS LYA detector spectrum at 0.3 AU, the "bare" detector regions are highlighted in gray.	30
Figure 13: Ly α detector expected countrate over 4 pxl (0.024 nm) spectral bin, vs spectral pxl number at 0.3 AU.	31
Figure 14: HI Ly α countrate integrated across the spectral line at 0.3 AU, versus dwell time.....	31
Figure 15: HeII detector expected countrate over 7 pxl (0.005 nm) spectral bin, vs spectral pxl number at 0.3 AU.	31
Figure 16: HeII 30.4 nm countrate integrated across the spectral line at 0.3 AU, versus dwell time.	31
Figure 17: METIS layout: on the left the optical elements and the bench are shown; on the right, there is a view of the instrument with baffles and enclosure.....	34
Figure 18: COR Optical path diagram.....	36
Figure 19: Scheme of the spectrometer configuration	37
Figure 20: Scheme of the spectro-coronagraph configuration	38
Figure 21: Configuration of the METIS instrument	39
Figure 22: Configuration with optical baffles removed and detail of the external occulter.....	39
Figure 23:Schematic of the IAPS detector.....	41
Figure 24:METIS High Level Electronic Architecture.....	42
Figure 25: METIS external envelope main dimensions.....	45
Figure 26. Flow diagram of the foreseen METIS integration activities.....	50
Figure 27: Modes of operation during the nominal extended mission.....	51

LIST OF TABLES

Table 1: COR's physical FOVs and spatial resolutions as a function of orbital position	23
Table 2: Wavelength ranges and pixel spacing for the three bands of the EUS spectrograph.....	26
Table 3 Spectral coverage of the three SOCS channels.....	29
Table 4: SOCS's slits angular and heliocentric positions	29
Table 5: SOCS's spectral resolution	29
Table 6: METIS Elements Performance Summary.....	32
Table 7: METIS Observational Modes	43
Table 8: Summary of METIS interfaces	45
Table 9. List of METIS sub-systems for which tests will be performed.....	46
Table 10. List of presently foreseen calibration activities at METIS element level.	48

1 Executive Summary

The *Multi Element Telescope for Imaging and Spectroscopy*, *METIS*, investigation is proposed in response to the Announcement of Opportunity (D/SCI – 23482) for submitting scientific investigations for the Solar Orbiter mission, issued by the European Space Agency (ESA) on October 18, 2007, in the frame of the joint ESA-NASA HELEX (Heliophysical Explorers) program.

The METIS design, conceived for the purpose of performing both EUV spectroscopy on the solar disk and off-limb and near-Sun coronagraphy and spectroscopy, is motivated by the aim of addressing the three key scientific questions identified as the focus of the HELEX program. These questions concern: the origin and heating/acceleration of the solar wind streams; the origin, acceleration and transport of the solar energetic particles; and the transient ejection of coronal mass and its evolution in the inner heliosphere (coronal mass ejections, CME's).

1.1 The Science

The investigation aims at providing crucial tests apt to verify the hypotheses and models, that have been developed primarily during the SOHO era, to address the following main questions on solar coronal physics:

- Is the slow solar wind originating according to more than one physical process and which is the level of contribution of the possible different sources of slow wind to the heliospheric wind observed 'in situ'?
- Is the magnetic field topology controlling the outflow velocity and composition of the fast and slow wind?
- Is the magnetic field controlling the emergence of the fast wind at the base of coronal holes?
- Do polar plumes and inter-plume regions have a role in channeling the fast wind?
- Is ion cyclotron dissipation of fast Alfvén waves the primary energy deposition process in the fast wind?
- Is the reconnection at the base of coronal holes responsible for the generation of waves and turbulence that energize the fast wind?
- Which is the nature of coronal heating in open and closed field regions?
- Which is the source of the seed particles of the Solar Energetic Particles (SEPs)?
- Which is the role of coronal shocks driven by coronal mass ejections in energizing SEPs?
- Which are the mass and magnetic fluxes carried out of the Sun during transient events?
- How does the evolution of the coronal magnetic field, inferred from the large-scale evolution of the outer corona, lead to trigger coronal mass ejections?
- How does the corona re-adjust after coronal mass ejections on medium-term time scales, ranging between 3 and 10 days, not yet established in the outer corona?
- How do the quiescent streamers evolve on time scales ranging between 3 and 10 days?

The crucial tests for addressing and solving these still open issues can be achieved by combining the instrument versatility with the uniqueness of the Solar Orbiter mission profile, which allows: a close approach to the Sun, thus leading to a significant improvement in spatial resolution; quasi co-rotation with the Sun, which allows to freeze for several days the outer corona in the plane of the sky and, thus, enable us to disentangle the evolution of coronal structures and solar rotational effects on medium-term time scales, and an out-of-ecliptic view of the Sun.

The METIS instrument, consisting of the COR, EUS and SOCS elements, is designed to combine and extend the spectroscopic and imaging capabilities of the SOHO, Hinode and STEREO spectrometers and coronagraphs in order to exploit at best the unique characteristic of the Solar Orbiter mission profile.

- It can simultaneously image the visible and ultraviolet emission of the solar corona (COR element) and diagnose, with unprecedented temporal coverage and space resolution (up to 8 times better than SOHO UVCS one), the structure and dynamics of the full corona in the range from 1.2 to 3.0 (from 1.6 to 4.1) solar radii from Sun center, at minimum (maximum) perihelion during the nominal mission, a region which is crucial in linking the solar atmosphere phenomena to their evolution in the inner heliosphere.
- It can observe key wavelength bands within the EUV/UV wavelength region 45-160 nm (EUS element), on the solar disk and off-limb out to 1.5 solar radii. This spectral region is dominated by emission lines from a wide range of neutral and ionized atoms, formed in the atmosphere of the Sun at temperatures ranging from 0.01 to 10 million K, so that an imaging spectrometer observing these lines is the only means by which chromospheric, transition region and coronal plasmas can be simultaneously observed and characterized,

giving the essential link between the Sun's surface and the 'in situ' measurements performed in the inner heliosphere by the Solar Orbiter and the Sentinels.

- In addition, it can combine both coronagraphy and spectroscopy (SOCS element) to observe the key wavelength bands within the EUV/UV wavelength region from 30 to 125 nm, in the geo-effective coronal region from 1.7 to 2.7 solar radii from Sun center, at the closest approach, a region which is crucial in meeting the HELEX science goals.

1.2 The innovation

For the first time METIS will be capable of obtaining:

- simultaneous imaging of the full corona in the visible and ultraviolet HI Ly α (121.6 nm)
- monochromatic imaging of the full corona in the extreme ultraviolet HeII Ly α (30.4 nm)
- spectral observations of the HeII (30.4 nm) line in corona
- simultaneous spectro-images of the corona in the OVI doublet, the HI Ly α (121.6 nm), HeII Ly α (30.4 nm), Fe XVIII (97.5 nm) lines, that can be performed simultaneously to coronal imaging
- first UV and EUV spectra out to 1.5 solar radii with a spatial resolution of the order of 160 km at the closest approach (a factor 5 better than SUMER).

These measurements will allow a complete characterization of the three most important plasma components of the corona and the solar wind in corona, in addition to the minor ions components.

The METIS suite has been designed following a highly innovative integrated approach, which takes advantage as much as possible of common subsystems for the three elements, such as the optical bench, the electronics, the DPU. A great advantage from the spacecraft point of view is that METIS makes use of a single aperture which is feeding the solar light to all the instrument elements, COR, EUS and SOCS. That is, a single aperture door is indeed needed instead of the two foreseen in the nominal payload for COR and EUS. The integrated design of METIS translates into a much reduced thermal load inside the payload. A further advantage, at the instrument level, is that the three elements, COR, EUS and SOCS, can be implemented using the resources nominally allocated on the spacecraft for the two elements, COR and EUS. This is a point of paramount importance because the scientific return which can be obtained by the METIS instrument is in this way greatly enhanced with respect to that expected in the case of the nominal payload, at essentially no additional cost with respect to the allocated resources.

1.3 The Instrument

The METIS suite consists of three different elements, each one dedicated to a specific scientific aim:

- a. COR, a visible-EUV coronagraph
- b. EUS, an EUV disk spectrometer
- c. SOCS, an EUV coronal spectrometer

The three elements share the same optical bench, electronics, and S/C heat shield aperture.

COR is based on a classical externally occulted design, in which light enters through an external occulter located at the outside panel of the S/C heat shield. The external occulter is supported by a suitable truss, which protrudes from the S/C instrument bay inside the heat shield; an extended external occulter can be inserted on the optical path, to allow observation of the solar corona also when the S/C is off-pointing from the Sun center. Three different coronal light wavelengths can be selected by a suitable filter mechanism: either visible, collected by a visible detector after being passed through a suitable polarizer, and/or ultraviolet (HI 121.6 nm or HeII 30.4 nm lines) collected by a suitable UV detector.

EUS is the portion of the spectroscopic element of METIS which includes the telescopes and all the related mechanisms. Light from the Sun disk passes through the METIS aperture on the S/C heat shield and is collected by a suitably coated telescope, which can be rotated around an axis passing through its vertex to scan the Sun disk along the East-West direction. A heat trap is located on the backside of this mirror to dissipate the heat from the Sun disk not reflected by the telescope. The EUV light reflected by the telescope is focused on the spectrograph slit plane; the slit can be selected, depending on the observation strategy, by a suitable mechanism. By means of another mechanism, a mirror can be inserted on the optical path to image selected portions of the solar corona, instead of the disk, on the spectrometer entrance slit. This allows to obtain spectroscopic measurement also on the corona, and not only on the Sun disk.

SOCS is the element with the insertable mirror that feeds the spectrometer box which includes the spectroscopic capabilities of METIS. The box consists of a fixed array of slits (the slits of interest are selected by means of a slit mechanism), a TVLS grating and a set of three independent detectors mounted on suitable position to collect three different interesting portions of the solar spectrum.

The spectrometer, shared by SOCS and EUS, allows to perform the spectral analysis of both the Sun disk and corona.

Summary of spacecraft resources required by METIS	
Optical Bench Size	1400(*)x755x200mm ³
Electronic units Size	220x250x350mm ³
Instrument mass (inclusive margin):	37.0 kg
Power consumption (nominal, inclusive margin)	50.2 W@28 V
Average Telemetry Rate	26.8 kb/s
	(*) 400mm are protruding through the sun shield

1.4 Instrument Operations and Scientific analysis

Of the three METIS elements, COR will obtain synoptic coronal images throughout the S/C orbit (at high cadence, 1 min, during the Nominal Observing Modes and at the lowest cadence, 1 hr, in the Time-Sharing Mode including aphelion). COR will also observe during S/C offset, thanks to the insertion of a larger occulter. EUS and SOCS share most of the optical path and thus are mutually exclusive. EUS will raster on disk, and off limb out to 1.5 R (when the S/C is off pointing) at a cadence of 1-3 h. EUS will observe only in Nominal Observing Modes. SOCS will obtain spectro-images of the corona in a sit and stare mode during part of the Nominal Observing Modes and during the Time-Sharing Modes close to perihelion, with a cadence of 1min. The METIS observations do not impose special requirements on the mission.

During the observation phase, the data products together with the Data Processing & Analysis Software, needed to obtain calibrated spectra and images, will be made available immediately to the METIS scientific team, and to the wider scientific community according to the ESA policy, in order to maximize the scientific return of the METIS investigation. Main scientific results and significant outreach material will be prepared and made available to ESA at regular intervals.

Operations, data reduction and scientific analysis will be supported by a team of approximately 25 scientists throughout the nominal mission.

1.5 The Consortium

The METIS investigation is proposed by an International Consortium under the responsibility of the Principal Investigator, Ester Antonucci, INAF-Osservatorio Astronomico di Torino (INAF-OATO). Experiment Manager of the METIS project is Giampiero Naletto, University of Padua and the METIS Investigation Scientists is Silvano Fineschi, (INAF-OATO). The METIS elements are in turn under the leadership of the following Co-PIs: Marco Romoli, University of Florence (COR), Daniele Spadaro, INAF- Osservatorio Astrofisico di Catania (EUS) and Dan Moses, Naval Research Laboratory, US (SOCS). The proposal is endorsed by the Italian Space Agency (ASI) as Leading Funding Agency.

The consortium is formed by the following Italian institutions: Istituto Nazionale di Astrofisica (INAF), the Universities of Florence, Padua, Pavia, Catania, the CNR – Istituto di Fisica della Materia (CNR-INFM), the Politecnico of Torino, and the following foreign institutions: Naval Research Laboratory (NRL), US, Max-Planck-Institut fur Sonnensystemforschung (MPS), Lindau, Germany, Laboratoire d'Astrophysique de Marseille (LAM), France, the Institute d'Astrophysique Spatiale (IAS), France, University of Athens, Greece, Royal Observatory of Belgium, Bruxelles, Belgium and Mullard Space Science Laboratory, UK. In terms of hardware contributions, NRL intends to provide the SOCS element, and is submitting to NASA a proposal in response to the NASA Focused Opportunity for Solar Orbiter, FOSO (deadline 31 January 2008), MPS intends to provide the two detectors of the COR element, LAM intends to provide the mirrors and mountings for COR.

This consortium has a long space experience. We only mention the recent and most relevant participations, consisting in the design, development and operations of the coronagraphs and spectrometers on SOHO (UVCS, LASCO and SUMER) and STEREO (SECCHI).

The financial status is described in the Financial Plan, which we asked to be confidential.

1.6 METIS data sheet

Name / acronym	METIS / Multi Element Telescope for Imaging and Spectroscopy
----------------	---

Objectives	Visible and EUV coronagraphy with the COR element
	Sun disk EUV spectroscopy with the EUS element
	Coronal EUV spectroscopy with SOCS

General description	Instrument suite consisting of three elements (COR, EUS, SOCS) mounted on a single optical bench, allocating common resources, and using a single aperture on the S/C heat shield.
----------------------------	--

Heritage	SCORE/HERSCHEL
	SUMER/SOHO
	UVCS/SOHO

Parameter	Units	Value / Description	Remarks	
<i>Sensor / detector</i>				
COR visible detector		1	APS	Integration mode
	Format		2048 × 2048	
	Pixel size	μm	25	
	Dynamic range	bit	16	
	Operating temperature	°C	-40	
COR UV detector		1	IAPS	Photon counting mode
	Format		2048 × 2048	
	Pixel size	μm	25	On the focal plane. The actual pixel size of the APS for the IAPS is 12 μm (see section 6.4.1.1.4 of EID-B)
	Dynamic range	bit	N/A	This detector works in photon counting mode
	Operating temperature	°C	20	
SOCS/EUS detector		3	IAPS	Both analog and photon counting regimes
	Format		2048 × 2048	
	Pixel size	μm	12	
	Dynamic range	bit	14	When working in analog mode (N/A in photon counting mode)
	Operating temperature	°C	20	
<i>Optics</i>				
Type			Different per each METIS element	
Unobstructed FOV	sr	2π	To be able to observe the very weak solar corona, no object can potentially scatter sun disk light inside the instrument aperture	
Energy passband		EUV to visible		
Pointing		+X _{Opt} S/C axis		
<i>Configuration</i>				
Physical Units	No	1		
Layout				
Location S/C		±Z panel	See section 3.3.5 of EID-B	
<i>Physical</i>				
Sensor Mass	kg	2.7	Mass of the five METIS detectors, including housing, mounts and doors	
Thermal Hardware Mass	kg	1.0	METIS total thermal H/W mass (conductive straps, thermal washers, thermistors)	

Harness Mass	kg	1.2	
Electronics Mass	kg	8.2	METIS Processing & Power Unit (MPPU)
Detector FEE	kg	1.1	For five METIS detectors
Total Mass	kg	29.6	METIS total mass, without contingency
Sensor dimensions		Ø70 mm × 55 mm	COR VD
		Ø90 mm × 75 mm	COR UVD
		Ø55 mm × 40 mm	EUS/SOCS
Harness Length	cm	~100	From the detector FEE to the MPPU
Electronics Dimension	cm ³	22 × 25 × 35	MPPU box envelope
<i>Power</i>			
Average	W	40.2	Before margins (25%)
Peak power	W	TBD	
Stand-by	W	TBD	
<i>Data rate / volume</i>			
Average data rate	bits/sec	27 k	
Peak data rate	bits/sec	TBD	
Minimum data rate	bits/sec	TBD	
Data volume /orbit	GByte	32	
Data storage	GByte	31	
<i>Thermal</i>			
Electronics Dissipation	W	37	MPPU dissipation, including 25% margin
Sensor Dissipation	W	13.2	Dissipation of all the detector FEE, including 25% margin
Heat load to radiator	W	130	Thermal power to be dissipated from the sun disk rejection mirror M0 and the heat absorber behind the EUS M1
Operating T range	K	293 ÷ 323	
Non-operating range	K	TBD	
Other requirements		TBD	
<i>Cleanliness</i>			
EMC requirements		TBD	
DC magnetic		TBD	
Particulate		TBD	
Molecular		TBD	
<i>Pointing</i>			
APE	arcmin	< 2	ILS
RPE		< 1 arcsec/10 s < 0.5 arcsec/10 s goal	ILS
<i>Miscellaneous</i>			
Mechanisms	No.	6	COR mechanisms: 1. Extended external occulter insertion 2. Filter exchange 3. Internal occulter alignment (during commissioning phase only) EUS mechanisms: 4. Scanning mirror 5. Coronal telescope insertion 6. Slit selector
Detector doors	No.	4	Single shot (TBC) 1 for COR, 3 for EUS/SOCS
Orbit requirements		N/A	
AIT/AIV requirements		TBD	

2 Scientific Objectives

The inclusion of instrumentation for EUV spectroscopy and near-Sun coronagraphy in the Solar Orbiter payload is motivated by the aim of addressing the three fundamental science questions identified as the focus of the joint ESA-NASA HELEX (Heliophysical Explorers) program, namely:

- What are the origins of the solar wind streams and the heliospheric magnetic field?
- What are the sources, acceleration mechanisms, and transport processes of solar energetic particles?
- How do coronal mass ejections evolve in the inner heliosphere?

Moreover, it will also:

- explore, at all latitudes, the energetics, dynamics and fine-scale structure of the Sun's magnetized atmosphere, as defined in the Solar Orbiter Science Requirements Document.

Aim of the METIS (Multi-Element Telescope for Imaging and Spectroscopy) investigation, that we propose for the Solar Orbiter, is to address the problems still open in the field of coronal and solar wind physics, relevant to the above main science questions. The basic scientific issues that are not yet fully clarified by the observations obtained with the in-flight spectrometers and coronagraphs of SOHO, Hinode and STEREO missions and the solar wind instrumentation on Ulysses, concern the physical processes that:

- generate the slow wind
- deposit energy in the regions of acceleration of the solar wind
- determine the elemental abundances in the extended corona and the solar wind
- supply the seed particles for solar energetic particles (SEP) acceleration;
- heat the outer solar atmosphere;
- lead to mass and magnetic fluxes carried out of the Sun in transient events.

In order to advance significantly in these fields, METIS will have the capability to:

- identify unambiguously the slow wind source via extensive high resolution observations, in space and time, of active region expansion, streamer formation and evolution;
- fully characterize the dynamics, kinetic temperatures and composition of the major plasma components, i.e., electron, hydrogen, helium and heavy ions, in the extended corona, site of the solar wind acceleration;
- detect populations of suprathermal ions that can become seed particles for SEP acceleration;
- study the velocity fields, temperature and composition of the solar atmospheric plasma at unprecedented high spatial, temporal resolution in order to eventually resolve the nature of the processes of energy deposition and dissipation;
- determine the 3D distribution and the directionality of the coronal mass ejections (CMEs).

2.1 METIS Investigation

By using a novel and unique approach which allows combining ultraviolet spectrometry, on disk and off limb (out to $1.4 R_{\odot}$), with UV spectro-imaging and visible and UV imaging coronagraphy capabilities, METIS will provide new and crucial observations, essential to address the above identified scientific objectives. METIS investigations are furthermore designed to benefit from the Solar Orbiter mission profile characterized by quasi-corotation intervals, close approach to the Sun and an out-of-ecliptic phase.

METIS significantly extends the spectroscopic and imaging capabilities of the spectrometers and coronagraphs operating at present in space by integrating the functions of three telescopes in a single instrument.

- **METIS COR**, a visible light and UV coronagraphic imager, for the first time obtains simultaneous visible and UV images of the full corona, which can provide a measure of the polarized brightness (pB) of the K-corona and the intensity of the neutral hydrogen H I Ly α 121.6 nm line, and, for the first time, can get monochromatic images of the full corona in the single-ionized helium He II Ly α 30.4 nm line. It can thus diagnose, with unprecedented temporal coverage and space resolution (down to about 2000 km, with an improvement of almost an order of magnitude relative to the SOHO coronagraphs), the structure, dynamics and energetics of the three main coronal and solar wind components: electron, hydrogen and helium. The COR observations in the range $1.2 - 3.0$ ($1.6 - 4.1$) R_{\odot} , at minimum (maximum) perihelion at 0.22 AU (0.3 AU), will provide i) the context for the EUS and SOCS spectroscopic off-limb observations, ii) trace the

early propagation of coronal mass ejections close to the limb and iii) investigate a region which is crucial for linking the solar atmosphere phenomena to their evolution in the inner heliosphere.

- **METIS EUS** element (Extreme Ultraviolet disk Spectrometer) is conceived to perform ultra-high resolution spectrometry of the upper chromosphere, transition region and inner corona, by observing 6 key wavelength bands within the EUV/FUV wavelength region 50 – 158 nm, on disk and off-limb out to 1.4 R_{\odot} . This spectral region is dominated by emission lines from a wide range of ionized atoms formed in the Sun's atmosphere at temperatures ranging from 0.01 to 10 MK, so that chromospheric, transition region and coronal plasma can be simultaneously characterised, describing the structure and dynamics of the Sun's magnetized atmosphere at all temperature regimes up to flare initial temperatures, altitudes and latitudes.
- **METIS SOCS** (Solar Orbiter Coronal Spectrometer) element has the capability of performing, in the same wavelength bands as the EUS, simultaneous spectroscopic observations at 4 different heliocentric distances in the outer corona, from 1.7 to 2.6 R_{\odot} at minimum perihelion (0.22 AU). Two aspects of the SOCS observations are of paramount importance: for the first time spectro-imaging of the outer corona in the most intense emission lines (e.g. H I Ly α 121.6 nm, O VI doublet 103.2,103.7 nm) is performed and the He II Ly α 30.4 nm intensity and profile is detected. Spectroscopy of the He II line is crucial for the characterization of the second most important component of the corona and solar wind and for the identification and diagnostics of the solar wind source regions.

The performances of the proposed instrument are in compliance with the coronagraph and EUV disk spectrometer described in the Solar Orbiter PDD, with the augmentation provided by the possibility of carrying out EUV spectrocoronagraphy (SOCS), that is a novelty in the design of METIS. Thanks to the close approach to the Sun during the early phases of the mission (0.22 AU perihelion), there is a significant increase in the spatial resolution of COR and SOCS with respect to the SOHO coronagraphs, as well as of EUS with respect to any previous EUV/UV spectrometer (at least a factor of five). Moreover, the spatial resolution of EUS is about a factor of two better than that of the TRACE imager. The spectral resolution of EUS is comparable to that of SUMER on SOHO, even better for the Ne VIII and C IV doublets wavelength regions, and of EIS on Hinode, whilst that of SOCS is comparable to that of UVCS on SOHO. The exposure times characterizing EUS observations (1-10 s), are an improvement with respect to those typical of SUMER (due to an average factor of three better throughput in our case). In the case of COR and SOCS, we have a cadence at least one order of magnitude shorter than that of the coronagraphs on board SOHO and STEREO, and of the spectrocoronagraph UVCS/SOHO, respectively. The shorter cadence of SOCS with respect to UVCS is also favoured by the multi-slit system inserted at the entrance of the spectrometer box, that allows observing simultaneously at 4 heights in the solar corona.

2.2 Mapping the origins of the solar wind streams

The knowledge of the detailed magnetic topology and dynamical behaviour of the source regions of the wind outflow are among the fundamental questions regarding the origin of the fast and slow solar wind streams.

2.2.1 The case of the slow wind

Whilst it is well established that the source of the fast wind resides in the large polar coronal holes and the debate is mostly concerning how the fast wind relates to the magnetic structure within coronal holes, the origin of the slow solar wind remains one of the outstanding questions arising in the post-SOHO era. At solar minimum there is evidence for an association of slow wind with the streamer belt and slow wind streams appear as a combination of a highly fluctuating component and of a quasi-stationary flow. Close to the Sun however, the slow wind appears to consist of at least two components (Wang and Sheeley, 1990; Strachan et al., 2002; Antonucci et al., 2005). There is evidence for a component emergent from the edges of coronal holes and flowing along the streamer boundaries, which shares nearly the same composition of the heliospheric slow wind, and thus it is probably its main source (Antonucci et al., 2006). In addition, slow wind leaks from the streamer regions and in this case its origin can be ascribed to quite different mechanisms.

Different models have been proposed for the source of these wind streams:

- a leakage from the closed field loops through reconnection at the cusp of the streamer due to coronal plasma pressure (e.g. Einaudi et al., 1999; Wiegmann et al., 2000);
- an outflow arising at the edges of coronal holes, due to intermittent reconnection of the super-radial open magnetic field lines with closed magnetic loops (e.g. Fisk et al., 1999; Schwadron et al., 1999; Fisk &

Schwadron, 2001), or to over-expansion of magnetic flux tubes (e.g. Wang and Sheeley, 1990, Antonucci et al., 2005);

- the existence of narrow regions of open field lines between multiple closed field configurations within the streamer belts (Noci et al., 1997; Wang et al., 2000; Noci & Gavryuseva, 2007).

During solar activity maximum the slow wind appears to emanate from small coronal holes and from active regions (e.g., Neugebauer et al., 2002) and to show in the heliosphere a larger degree of turbulence and a higher helium abundance than the solar minimum slow wind.

METIS can assure a full spatial coverage of the region where the slow wind is accelerated, from the limb outwards, by means of combined EUS and COR observations, which are also co-spatial from 1.2 to 1.4 R_{\odot} at least in the first phase of the mission. This will allow to map for the first time with high accuracy and unprecedented space resolution the outflow velocity, composition, density of the slow wind close to limb, in order to identify the predominant mechanism for plasma leakage from streamers and assess the relative role of the slow wind coming from the edges of coronal hole and that generated within streamers. At present reliable slow wind measurements have been performed only above 1.7-1.8 R_{\odot} .

The observations with METIS EUS will provide high spatial, temporal and spectral resolution EUV spectroscopic data on the disk and off-limb that, together with EUV images and magnetic topology data from VIM, can characterize the plasma state (temperature, density and flow structure, and chemical composition) in closed and open field regions, which all together may contribute to the slow solar wind streams; detect plasma ejections from the sites where reconnection between open flux and closed loop may occur, also quantitatively evaluate differences in the amount of energy released with respect to the case of the high-speed streams. The observations with METIS COR will provide high spatial resolution outflow velocity maps of the hydrogen and helium components and the electron density maps of the slow wind in corona.

2.2.1.1 Slow wind sources identified with He abundance measurements

METIS will obtain data on the He composition from the limb to 2.6 R_{\odot} , or at larger distances later in the mission, that has never been measured yet, and will provide the definitive test to ascertain which of the slow wind coronal source/s is/are predominant in the heliospheric slow wind.

The determination of the helium abundance in the extended corona is indeed strictly related to the issue of the origin of the slow solar wind. According to UVCS observations, the core of solar minimum quiescent streamers shows a strong depletion of five times ionized oxygen. This effect can be interpreted either in terms of gravitational settling of heavier ions in a coronal plasma confined by closed field lines (Raymond et al. 1997), or in terms of dynamic stratification because of reduced Coulomb dragging of the ions in the slow wind (Noci et al. 1997, Marocchi et al. 2001). This latter effect can occur in magnetically complex streamers, consisting of sub-streamers separated by open field lines channelling slow wind streams.

METIS allows a comparative study of the helium abundance structure in streamers with the well-known oxygen abundance structure, which will result to be crucial in order to distinguish between the above different interpretations of core dimming. In fact, on the one hand helium is lighter than oxygen and thus less affected by gravitational settling, and on the other hand, its drag factor in the slow wind is the least favourable (Geiss et al. 1970).

METIS COR will obtain monochromatic imaging of the outer corona in the most intense ultraviolet lines, the Ly α lines of H I and He II, in order to derive velocity and abundance maps of the hydrogen, helium components in the streamer regions. METIS SOCS will obtain overlapping velocity and abundance maps of the hydrogen, helium and oxygen components in 4 stripes of the streamer region. The comparison of He structure and evolution and the OVI structure and evolution obtained with SOCS will allow to ascertain the role of the slow wind in determining the composition anomaly in the streamer core discovered by the UVCS and eventually in identifying one of the possible slow wind sources.

2.2.1.2 Role of magnetic topology in controlling the solar wind properties

METIS investigation will allow us to test the hypothesis that the outflow velocity of the coronal plasma is controlled by the divergence of the flux tubes. It will indeed be possible to assess the role of the coronal magnetic topology and its evolution by measuring simultaneously the helium abundance and the wind velocity in corona.

The wind velocity is supposed through experimental evidence to be directly related to the expansion factor of the magnetic flux tubes channelling coronal expansion within the first 3 solar radii (Wang and Sheeley 1990, Antonucci et al. 2005, Antonucci 2006). On the other hand the heliospheric wind velocity appears to be correlated to the heliospheric helium abundance (Aellig et al. 2001). The abundance variations can therefore denote temporal or space differences in the expansion factor of the open magnetic fields, and can be considered a signature of the magnetic topology in corona. Determination of the helium abundance thus will provide a decisive test of the role of the flux tube divergence in controlling the coronal wind properties.

METIS COR will obtain sequences of visible light images, monochromatic H and He coronal images to determine the evolution of the outflow velocity and the He abundance relative to hydrogen. These measurements will lead to infer the coronal magnetic topology and its evolution.

2.2.2 The case of the fast solar wind

2.2.2.1 Role of the magnetic structure in controlling the solar wind emergence

METIS observations will test the hypothesis that the emergence of the high-speed solar wind, originating at the base of large polar coronal holes present at solar minimum, is controlled by the chromospheric magnetic structure.

Evidence for emergence of the fast wind from coronal regions located roughly along the boundaries of the magnetic network cells (Hassler et al., 1999) and in association with coronal funnels (expanding magnetic field structures rooted in the magnetic network lanes) has been found (Tu et al., 2005). The ultra-high spatial resolution of the METIS EUS spectrometer, achieved during the closest approach at 0.22 AU, that will improve by at least a factor of 5 relative to any previous EUV/UV spectrometer, will allow an extremely accurate spatial association of the Doppler shift of the initial fast solar wind with the network structure as measured by VIM, thus verifying in a definitive way whether the magnetic network is indeed controlling the emergence of the fast wind.

In order to assess the dependence of the emergence of the fast solar wind on the chromospheric network, METIS will perform high spatial, spectral and temporal resolution EUV spectroscopic observations of coronal holes as seen on the 1\disk. Measurements of the Ne VIII resonance doublet lines (77.0, 78.0 nm), expected with a resolution apt to detect line-of-sight velocities around 1 km/s (by line centroiding), and with a spatial resolution of 160 km (pixel size) at 0.22 AU will be crucial. These lines form at the top of the transition region in coronal holes, at temperatures ~ 0.6 MK, so that the initial start of wind outflow can be detected. The EUV spectroscopic observations must be carried out with both VIM and EUI on board Solar Orbiter, in order to correlate Doppler-velocity and radiance maps in different spectral lines with the magnetic field extrapolated from high resolution photospheric magnetograms and the detailed fine structure coronal morphology of the examined regions.

Although the end of the nominal mission, when the out-of-ecliptic phase will allow the best conditions for spectroscopy of the high latitude coronal holes (higher line-of-sight component of the outflow velocity), will most probably occur around maximum of activity, a significant out-of-ecliptic latitude of 20 degrees will be reached in Feb. 2020 (P4). Moreover, during the extended phase, when the polar coronal holes will form again, it will be possible to exploit the joint effect of high spatial and spectral resolution observations and best line-of sight effect conditions.

2.2.2.2 Identifying the solar wind sources on the basis of the elemental composition

Another approach that METIS investigations will adopt, in order to allow us to trace the fast solar wind streams back to their solar origins, is based on a comparison of the heliospheric and coronal wind composition, exploiting the combined Sentinels 'in situ' and Solar Orbiter 'in situ' and remote sensing observations.

Spectroscopic measurements of elemental abundances in the transition region and the low corona layers of coronal holes will be performed at high spatial resolution by METIS EUS, in association with the magnetic field topology determined by VIM. Elemental composition results will be used to investigate the fractionation processes occurring in open magnetic structures (cf. Laming, 2004). Coronal composition will also be compared with in-situ composition measurements from both Sentinels and Solar Orbiter, particularly during quadratures and conjunctions, in order to

unambiguously link the solar wind streams to their solar sources. The combination of high-resolution remote sensing with in-situ measurements will be performed at best during the co-rotation phase, early in the mission, due to the highest spatial resolution achieved because of the proximity of the Orbiter to the Sun (expected perihelion between 0.226 and 0.254 AU).

2.2.2.3 Determining the role of plumes in the generation of the fast wind

METIS will help to address the question concerning the role played by coronal plumes in the fast wind outflow.

Following the path of the fast solar wind once emerged from the transition region, the next question that has to be answered is whether the fast wind is channelled outwards along plumes or interplume regions. This is a long-lasting question that can be solved by combining co-spatial METIS EUS spectroscopic observations and COR coronagraphic images in the polar regions, close to the solar limb. Outflow velocity will be determined by measuring the Doppler dimming of HI Lyman α (e.g., Giordano et al., 2000; Teriaca et al., 2003, Gabriel et al., 2003) simultaneously with the electron density from polarized visible light coronal images. The analysis of spectroscopic data will provide information on the plasma properties such as density, temperature and composition and outflow velocity of the oxygen ions (via Doppler dimming) at the base and along polar plumes and in the interplume regions.

The same observations will cast light on the nature of plumes as well. At present, there is controversy on the nature of the elongated radial features observed in the outer corona in visible light and UV emission and defined as 'polar plumes'. Are they the extension of the features observed lower down close to the disk, or more simply tiny threads with larger density that are by chance aligned along the line of sight? These alternatives can be verified by observing plumes both in a rotating and in an almost non-rotating Sun. In the latter case the changes in morphology are only due to the 'plume' intrinsic evolution. During the quasi-corotation phase of the mission the plumes can indeed be seen on the plane of the sky, owing to the small inclination angle with the ecliptic of the spacecraft orbit, and their observed morphology is negligibly affected by solar rotation

2.3 Understanding the plasma heating and acceleration of the solar wind

2.3.1 Energy deposition in the fast solar wind via ion cyclotron dissipation of fast Alfvén waves.

METIS will provide the definitive proof that the energy deposition needed to accelerate the fast solar wind beyond the sonic point to reach the asymptotic speed up to 800 km/sec, occurs via ion cyclotron dissipation of fast Alfvén waves by obtaining spectroscopic measurements of the He II 30.4 nm line in the region where the fast wind is accelerated.

The heating and acceleration of the solar wind remains a basic unsolved problem in solar and heliospheric physics. SOHO has indeed provided the first observations of outflow coronal regions where the solar wind is accelerated. The highest acceleration of the fast solar wind emanating from coronal holes occurs beyond the sonic point between 2.0 and 3.0 R_{\odot} (e.g. Telloni et al., 2007). The unexpectedly broadened OVI 103.2, 103.7 nm doublet observed where the wind acceleration is highest, is ascribed to an extremely broad ion velocity distribution, associated with a kinetic temperature of the order of 10^8 K. These results have raised great interest since the observed line broadening must be interpreted as a signature of the energy deposition in the outflowing wind.

The suggestion is that collisionless wave dissipation is acting, with ion cyclotron resonance damping of the high frequency part of the Alfvén spectrum being the most probable mechanism to explain the observed effect (e.g., Cranmer 2002). The transfer of mechanical energy from the inner atmosphere can only occur by low frequency Alfvén waves, owing to the strong gradients and structuring in the chromosphere and transition region, and is then distributed to higher frequencies through turbulent cascade in the outer corona, where can be dissipated via wave-particle interactions. This explanation for the acceleration of the fast wind can be definitely proved by measuring the emission of ions with different charge-to-mass ratios. This is because dissipation can occur when the Alfvén wave frequency is of the order of the ion cyclotron frequency, which is proportional to the charge-to-mass ratio Z/A . Essential in this respect is then the observation of the intensity and profile of the He II 30.4 nm line ($Z/A = 0.25$), in addition to that of the O VI ions ($Z/A = 0.31$), and of the protons ($Z/A = 1$), whose outflow velocity and velocity distribution can be deduced from the intensity and width of H I Lyman series lines, due to the high rate of charge exchange between protons and neutral hydrogen.

*In order to definitely prove the above hypothesis, the high resolution UV spectroscopic observations of the extended corona expected from **METIS (EUS and SOCS)** from the solar limb up to 2.6 solar radii, and even farther later in the mission, will measure outflow velocities, via Doppler dimming, and the line-of-sight velocity distribution of different ions with different charge-to-mass ratios, in particular H I, He II, and O VI.*

*In addition, **METIS COR** will obtain data on the visible polarized brightness (pB) of the K-corona, used to derive the electron density distribution in the same regions of the extended corona, and narrow-bandpass images of the whole extended corona from 1.2 to 3.0 R_{\odot} in the HI 121.6 nm Ly α line and in the single-ionized helium HeII 30.4 nm Ly α line, to derive the density distribution and radial outflow velocities, through Doppler dimming, of the hydrogen and helium components. The acquisition of information on the outflow velocities of both solar wind plasma components all over the extended corona will be crucial to clarify the nature of the mechanism of energy deposition in terms of the above discussion on Alfvén wave dissipation, and quantify the degree of energy transferred to the major constituents of the solar wind.*

2.3.2 Reconnection of closed and open structures as sources of waves and turbulence to heat the fast solar wind

EUV spectroscopy and imaging will be capable to detect magnetic reconnection in the transition region and corona, e.g., by the high cadence (5-10 s exposures) observation of plasma jets or explosive events as seen in the heavy-ion Doppler motions believed to mark the reconnection-driven plasma outflow (Innes et al., 1997). The detection of these events in regions with open magnetic configuration is very important, since Tu et al. (2005) proposed that the reconnection resulting from interactions of small closed loops and the open structures supplies energy in the form of waves and turbulent flows to the nascent fast solar wind.

2.3.3 Which is the origin of turbulence in the solar wind?

METIS COR will be able to provide, during quasi-corotation intervals, time series longer than 2-3 days of visible and UV images of the same portion of the extended corona, well suitable to calculate power spectra and relevant frequencies of the fluctuations occurring in the inner heliosphere.

Observations have shown the solar wind to be a highly turbulent and dynamically evolving magnetofluid, but the sources of the turbulence and fluctuations are not well understood yet. Although simulations show that, in a highly stratified atmosphere, the nonlinear interactions of Alfvén waves launched from the photosphere are able to generate and sustain an incompressible turbulent cascade, which displays the observed Alfvénicity in the solar wind, the efficiency of turbulence in transporting energy to the dissipative scales is, however, still unclear. We know that the slope of the Alfvén energy spectrum at different coronal heights evolves with distance, owing to expansion and driving effects, affecting the radial dependence of dissipation. However, the initial spectrum of Alfvén waves in the photosphere cannot be constrained by in-situ data collected in the far solar wind, since local processes contribute to its shaping there (Verdini and Velli, 2007).

Remote-sensing observations of EUV and visible coronal emission, at high spatial resolution and temporal cadence, during quasi-corotation and over a range of distances covering from close to the solar surface out to 2-3 R_{\odot} will help in constraining the amplitude of the turbulence spectrum, with relevant implications on the role of turbulence in the acceleration of the solar wind and heating of the corona, as well as in characterizing the plasma state in active region coronal loops and open field regions that may contribute to the fluctuations and fine structures propagating in the solar wind. Distinguishing pure temperature effect from turbulence amplitudes via a number of spectral line profiles acquired off-limb by EUS and in the inner heliosphere by SOCS will be of paramount importance.

The comparison of remote-sensing with in-situ measurements should be particularly well-suited to identify the solar source regions of the fluctuations and fine structures observed in the wind.

Moreover, extended observations of the same coronal region during quasi-corotation intervals and the diagnostics of distribution function anisotropy will also set constraints on the wave-particle acceleration in the corona. In the acceleration region large anisotropies may be due to the cooling of the distribution function in the direction parallel to the magnetic field lines in comparison to the perpendicular one, so that the region of maximum anisotropy provides an important information about the details of the wave-particle interactions.

2.4 Which are the sources of solar energetic particles (SEPs)

METIS will provide definitive evidence for the acceleration of solar energetic particle events (SEPs) by part of CMEs by means of spectro-imaging of the region covering the early propagation of the transient coronal events.

There is mounting evidence that coronal mass ejections (CMEs) that are efficient accelerators of SEPs are generally preceded by another CME within the previous 24 hours, with a mean delay of 11 hours (Gopalswamy et al., 2004). The preceding CME must also have been fast, i.e. with speed greater 700-800 km/s, so that it would have driven a shock in the low corona. The suggested scenario then is: this first CME supplies a population of suprathermal ions (around 0.1-1% of total number of particles) whose energies are somewhat higher than the local plasma, that can become the seed particles for SEP acceleration by the second CME. These suprathermal particles are favoured in the acceleration of SEPs, since their higher energy gives them a “head start” over the local plasma population. Studying the time-varying composition of the suprathermal particles in the inner heliosphere will give us critical insights into what material is actually being accelerated by fast CME-driven shocks.

METIS SOCS will attempt to detect these suprathermal populations, spectroscopically, close to the Sun, in coincidence with the observations of CME shocks profiles. Deviations of line profiles from a Maxwellian into a kappa distribution (with kappa values of order 2-3) will have to be observed in the H I Ly α and Ly β lines and in the O VI resonance doublet, against a coronal background most likely formed by Thompson scattering (and broadening) of the disk line profile by coronal electrons. Preliminary simulations of expected coronal line profiles show that $10^4 - 10^5$ total counts in the line will be necessary to distinguish any SEP seed particle population. High signal-to-noise, low straylight spectroscopic observations with sufficient signal to measure line broadening due to kappa distributions are required, together with a temporal resolution of some minutes in order to follow the time evolution of the populations.

The SOCS observations will be combined with the EUS spectroscopic data on disk and COR visible-light/UV coronal images that will provide the timing necessary to distinguish flare sites vs. CME-driven shocks accelerating energetic particles, and the wide aperture long-term observations suitable to monitor sources that can be subsequently seen in-situ.

2.5 Investigating the evolution of coronal mass ejections in the inner heliosphere

The most energetic manifestations of solar activity and the drivers of the most severe space weather effects are the giant disruptions of the Sun’s magnetic field observed as a coronal mass ejection (CME). During solar maximum, CMEs dominate the structure and dynamics of the heliospheric field and plasma at all latitudes. They are often associated with filament/prominence eruptions or flare events (e.g., Gopalswamy et al., 2003).

METIS is expected to play a fundamental role in investigating how CMEs erupt and evolve in the inner heliosphere since it provides the capability to observe the early CME propagation from very close to the limb (from $1.2 R_{\odot}$ in the position of closest approach). In addition, this capability during the corotation phase provides an unprecedented opportunity not only to investigate the triggering of the eruption but also the evolution prior to the CMEs onset and the reconfiguration of the magnetic fields following the coronal mass ejection.

The observations obtained with METIS EUS will lead to:

- Identification of CME onsets, through detection of ejecta and coronal dimming events –
High spatial, spectral and temporal observations of pre-flaring filaments is essential to map the evolution of the physical parameters of the filament and its environment. Pointing EUS on the disk will allow observing lines from the chromosphere to corona, in such a way to temporally characterise the thermal properties of the filament and the surrounding corona, prior and during the initial phase of eruption. Density diagnostic will also be possible, allowing disentangling mass motions from density variations, both responsible for intensity variations. EU/HRI high cadence images will be used as context, to picture the morphology changes at different temperatures, completed by VIM/HRT photospheric magnetic field measurements used for coronal extrapolations.

With METIS COR will be possible to

- Observe the full sequence of pre-eruption, eruption and propagation of a coronal mass ejection, as well as the reconfiguration of the extended corona following the CME during a quasi-corotation interval -
This would be instrumental to: (i) identify the mechanism(s) driving the eruption among the several ones proposed (e.g., Antiochos 1998, Forbes & Isenberg 1991, Low 1996); (ii) ascertain whether the main source of flux injection

into the heliosphere is indeed residing in the outer corona; (iii) study the restructuring of the global corona following mass ejections.

These observations need to be performed at very high space resolution in order to resolve the fine structure of the magnetic fields, plasma density and flows, when evolving toward the disruption leading to a coronal mass ejection. During most of the nominal mission corotation occurs at perihelion (0.226 - 0.254 AU), therefore an improvement of almost one order of magnitude in space resolution relative to the present SOHO coronagraphs can be easily achieved.

2.5.1 Study of the longitudinal structure of the active Sun

The out-of-ecliptic observations can provide information on the longitudinal extent of the magnetic system involved in coronal mass ejections. In conjunction with observations performed in the ecliptic, this allows the reconstruction of the three-dimensional geometry of these events and the evaluation of the total mass and magnetic flux injection into the heliosphere, all along the streamer belt. In case high inclination with respect to the ecliptic is reached when the Sun is active, the most interesting scientific objective is that of investigating the 3-D geometry of mid-, high-latitude coronal mass ejections. The latter have been identified during the last maximum with the LASCO coronagraph and occur when the solar magnetic fields reverse at the poles.

2.5.2 Spectroscopic detection of cool ($\sim 10^4$ K) plasma ejected in the inner heliosphere

Spectroscopic measurement in the off-limb corona will be also used to diagnose with high spatial resolution the filament material once erupted, by the observations of chromospheric lines (e.g., C III 97.7 nm), unusual in corona, in the CME core (e.g., Ciaravella et al., 1997; Ventura et al., 2002). The combination of EUS and SOCS will fully cover the distances from the disk up to 2.6 solar radii. Thanks to the presence of a multi-slit spectrometer, it will be possible for the first time to separate between temporal and spatial variations of plasma temperature, densities, abundances, etc. inside a CME, providing for instance information on the evolution of the CME bubble plasma temperatures and of the energy carried by the CME. The estimate of line-of-sight velocities (from line Doppler shifts) and radial velocities (derived with the Doppler dimming techniques, also using UV coronagraphic images) in different parts of the CME at the same time will give important information on the 3D structure and expansion of the CME bubble (cf., Antonucci et al., 1997).

2.5.3 Spectroscopic detection of plasma heated by reconnection events after the CME front transit

There have been also reports of current sheet (CS) detections in the extended corona, from observations of CME events by UVCS and LASCO (see, e.g., Akmal et al., 2001; Ciaravella et al., 2002; Raymond et al., 2003; Bemporad et al. 2006, 2007; Rakowski et al., 2007). CSs correspond in general to ray-like bright structures in the white light LASCO images, and have been identified in UVCS data from the presence of unusual emission in the high temperature Fe XVIII ion (97.4 nm), attributed to plasma heated by reconnection. The presence of a multi-slit spectrometer (SOCS) will allow the detection of this and other UV lines, coming from the same structure, at different altitudes at the same time, playing a fundamental role in the study of post-CME current sheet evolution.

2.5.4 Observation of plasma shock heating at the CME front

A comprehensive determination of the properties of shocks near the solar origin is essential if we are to make progress on understanding and predicting SEPs. On the other hand, direct imaging of coronal shocks remains in fact an outstanding observational challenge (Gopalswamy et al., 2001; Mann et al., 2003).

UV spectral observations of CME-associated coronal shocks have been able to solve this problem, providing both spatial resolution and unique diagnostics for the physical processes in coronal shocks. The main indicator of the shock passage in the UV spectra is represented by the sudden dimming and broadening of the O VI 103.2, 103.7 nm line profiles together with simultaneous brightenings of the spectral lines from heavier ions, such as Si XII 49.9, 52.1 nm and Mg X 61.0, 62.5 nm (Raymond et al., 2000; Mancuso et al., 2002; Ciaravella et al., 2005). The SOCS multi-slit spectrometer of **METIS** is designed to observe these lines, emitted by the coronal plasma compressed and heated by the transit of the fast and wide front of the CME, at different radial heights at the same time, yielding important constraints on physical plasma parameters, such as the coronal plasma β and local Alfvén speed (Mancuso et al., 2003), and the relationship between the dynamics of the shock and the associated CME (Mancuso & Raymond, 2004; Mancuso, 2007).

A direct observation of a CME-driven shock and the measurement of its properties and their correlations with SEP events (Reames et al., 1997) could be thus very useful in establishing the necessary or sufficient conditions for shocks to accelerate ambient solar wind or suprathermal ions to SEPs.

2.6 Determining the nature of the energy deposition and dissipation mechanisms

EUS, the EUV/FUV disk spectrometer of **METIS**, can greatly help to study the dynamics of the outer solar atmospheric plasma at high spatial (at perihelion a factor of five better than any previous EUV/FUV spectrometer), spectral (up to $\sim 47,000$, better than that of SUMER on SOHO) and temporal (1 to 10 s exposures) resolution, in order to determine the nature of the coronal heating mechanisms.

The heat source that causes the hot corona has proved elusive. It is well established however that there is a direct link between magnetic field strength and heat input in the corona. The heating of quiet and active regions is likely caused by the same mechanisms, with active regions receiving more heat simply because the concentration of intense magnetic flux is higher. Dissipation of magnetic waves and direct magnetic dissipation of electric currents in intense current sheets are the two most probable agents for coronal heating (see, e.g., Klimchuk, 2006). In order to assess the role of the two main dissipation processes, it is necessary to reach the capability of measuring coronal magnetic waves, and magnetic turbulence due to their decay, and of identifying, indirectly, current sheets and their effects.

The optical design and technical characteristics of **EUS** are suitable to:

- derive the plasma temperature, density, flow velocity, non-thermal energy input and chemical composition in transition region and coronal structures with different magnetic configuration (open coronal holes and funnels, closed loops and prominences), linking them with the magnetic field values derived at different spatial scales (both directly and through extrapolations) from **VIM** observations;
- determine, on the basis of the above plasma parameters collected in a wide range of magnetic loops with different spatial scales, whether heating is spatially localized or uniform, and time steady or transient (and probably impulsive);
- make a step ahead in resolving the geometry of fine elemental loop strands (Aschwanden et al., 2002; Reale et al., 2007), and define the possible multi-temperature nature of such structures and their transversal expansion in the corona, giving insight to the level of the tangling of the magnetic flux tubes (Lopez Fuentes et al., 2006);
- detect and characterize waves in closed and open structures (see, e.g., De Pontieu et al., 2007), looking for signatures of their dissipation in the transition region and low corona, with a corresponding evaluation of the energy released to heat the solar plasma;
- investigate the role of small scale magnetic flux emergence in energizing the above laying layers (see, e.g., Galsgaard et al., 2007);
- detect, measure and characterize dynamic and energetic signatures of reconnection in the chromosphere, transition region and low corona, driven by magnetic field evolutionary processes - for instance, brightenings (Harrison et al., 1997), flows and jets (Innes et al., 1997) and plasma evaporation (Klimchuk, 2006) -, in close coordination with **VIM**.

All the above measurements will greatly benefit from the cooperation with the **EUI** imaging instrument, in both full disk and high resolution mode.

We would finally stress the importance of improving the observations of elemental abundances, in order to investigate in more details fractionation processes (for instance, the FIP effect, cf. Laming, 2004) and possible variations in the chemical composition of the outer solar atmosphere with respect to the photosphere, or among regions with different physical properties in the same layer (e.g., Spadaro et al., 1996). All this could also give us a clearer picture of the propagation of waves and turbulence in the solar atmosphere, and of course get us closer to an understanding of coronal heating and activity.

2.7 Structure and evolution of streamers

METIS will unveil the evolution of streamers on time scales ranging from 3 to 10 days for the first time, during the quasi-corotation intervals..

The extended observation at the limb of the same portion of corona is essential to address the study of streamer structure, evolution and dynamics. This will focus, depending on the mission launch date, either on the quiescent, slowly evolving streamer belt or on the rapidly varying active streamers. The investigation of the interrelation of solar wind acceleration region and magnetic topology of the flux tube guiding the expansion necessitates as well long-term observations. The opportunity to freeze a streamer section at the limb offers, in addition, the possibility of increasing dramatically the statistics, being, in this case, only limited by the intrinsic evolution of the structure and not by solar rotation. A significant increase in statistics is then coupled with the possibility of observing at high spatial resolution; this allows us to resolve the fine structure and relevant dynamics in the slow wind coronal source regions. This kind of studies requires the simultaneous knowledge of the electron density and morphology of the corona, by observations in visible light, and of the radial flow velocities, obtained with better accuracy and detail from images of the ultraviolet H I and He II emission, by Doppler dimming techniques.

A coronagraphic view of the longitudinal/azimuthal structure of the global corona will be possible for the first time during the out-of-ecliptic phase, after the end of the nominal mission, when the inclination angle with the ecliptic increases from 30° to 34° while perihelion increases from 0.344 to 0.375 AU. This completely new perspective will greatly impact on the study of large-scale structures of solar corona. If this phase occurs during solar minimum, from high latitudes the Orbiter views the streamer belt running at low-latitude, or close to the equator, as an approximately continuous annular structure around the solar disk. Furthermore, the out-of-ecliptic vantage point is indeed providing another means to observe the corona not affected by solar rotation. When the morphology is relatively simple and the relevant coronal features are at low-latitude, or close to the equator, their intrinsic evolution can indeed be easily separated from rotational effects, if viewed from high-latitudes.

Another interesting aspect concerns the possibility to study the dynamics of coronal expansion all around the streamer belt. During solar minimum, slow solar wind studies would be privileged, since their supposed low-latitude and equatorial sources are predominant on the plane of the sky. It would then be possible to (i) assess the contribution to the slow wind of sporadic reconnection events, such as the coronal blowouts, and (ii) evaluate the total mass and magnetic flux injection into the heliosphere all along the streamer belt. The last aspect will represent a step forward, crucial to the understanding of the suggested secular variations of the heliospheric magnetic flux and of the relevant influence on the global Earth climate.

2.8 Solar Orbiter Mission Requirements

The achievement of the scientific objectives listed above critically depend on a series of points that are described here.

2.8.1 Solar Orbiter spacecraft performance

It is important that METIS is placed on the $-Z$ side of the spacecraft looking at the centre of the solar disk (spacecraft coordinate system), in order to allow SOCS to observe the West side of the solar corona, more interesting in the study of the temporal evolution of coronal structures.

In addition, it is important that the optical axis of the spacecraft coincides with the boresight of METIS, ruled by the COR element. This in order to guarantee that the inner boundary of the FOV of COR at minimum perihelion is as close as possible to solar limb. Also the maximum spacecraft off-setting at 0.22 perihelion should be within the limits stated in the RD1, in order to avoid that the disk light enters the COR optical path, with the consequent closure of the entrance door of the instrument.

Finally, the high spatial resolution of the instrument, in particular of the EUS element, relies on the alignment stability of the spacecraft, that should be within 1 arcsec over the typical exposure time of the spectrometer, i.e., 10 s.

2.8.2 Solar Orbiter orbit

METIS investigation will greatly benefit from all the nominal characteristics of the planned orbit, i.e., close approach to the Sun, quasi-corotation and out-of-ecliptic phase. The quasi-corotation intervals are crucial in order to study in details and on a mid-term (3-10 days) temporal scale the magnetic topology, chemical composition, dynamical behaviour and evolution of the source regions of the wind outflow. Moreover they are important to observe the full sequence of pre-eruption, eruption and propagation of a coronal mass ejections in the inner heliosphere, as well as the reconfiguration of the corona following the CME.

2.8.3 Other Solar Orbiter payload elements

Studies of the initial acceleration of the solar wind streams in the relevant source regions seen on the solar disk, together with those related to the nature of the coronal heating mechanisms, will be more fruitful if jointly carried out with the EUI and VIM instruments, apt to provide data on the morphology and evolution, and on the photospheric and coronal (by extrapolation) magnetic fields, of the target regions. In this context a knowledge with great accuracy of the co-alignment of METIS, specifically EUS, with these units is important.

2.8.4 Ground segment

It is very important to exploit at maximum the entire available telemetry throughput for high cadence on disk observations of CMEs and transients, and of magnetic reconnection signatures also. Getting the entire FOV of COR, in particular during the phases of the orbit at heliocentric distances around 0.5 AU or larger, is also important to complement the FOV of the heliospheric imager planned in the Solar Orbiter payload, as well as for the simultaneous remote-sensing observation of heliospheric regions sampled in-situ by the Sentinels.

3 Instrument Performances

The analysis of the expected instrument performances shows how METIS matches the observational requirements derived by the scientific objectives presented in the preceding section.

3.1 COR: Visible light and UV Coronagraphic-Imager

COR is a Visible light and UV Coronagraphic Imager, observing the full corona in three wavelength bands:

1. Linearly polarized visible-light, broadband: 500-600 nm
2. UV HI Lyman- α , 121.6 nm; narrowband: $\lambda/\Delta\lambda=10$
3. EUV HeII Lyman- α , 30.4 nm; narrowband: $\lambda/\Delta\lambda=10$

3.1.1 Instrument Observational Parameters and Sensitivities

Field of View: COR has an annular field-of-view (FOV) with angular extension of $\pm 3.5^\circ$ and with 13 arcsec spatial resolution. The physical heliocentric distances of the FOV vary along the orbit and through the mission.

Heliocentric distances (AU)	FOV in heliocentric heights (Ro)	Resolution on the plane of the sky (km)
0.22	1.2 - 3.0	2000
0.3	1.6 - 4.1	2700
0.5	2.7 - 6.8	4550
0.8	4.3 - 11	7300

Table 1: COR's physical FOVs and spatial resolutions as a function of orbital position

The FOV at perihelion (1.2-3 Ro) and at 0.5 AU (2.7-6.7 Ro), heliodistance which includes the Solar Orbiter nominal observing modes during the initial phase of the mission, are shown in Figure 1. The FOV at maximum perihelion, at the end of the nominal mission, falls within these two cases.

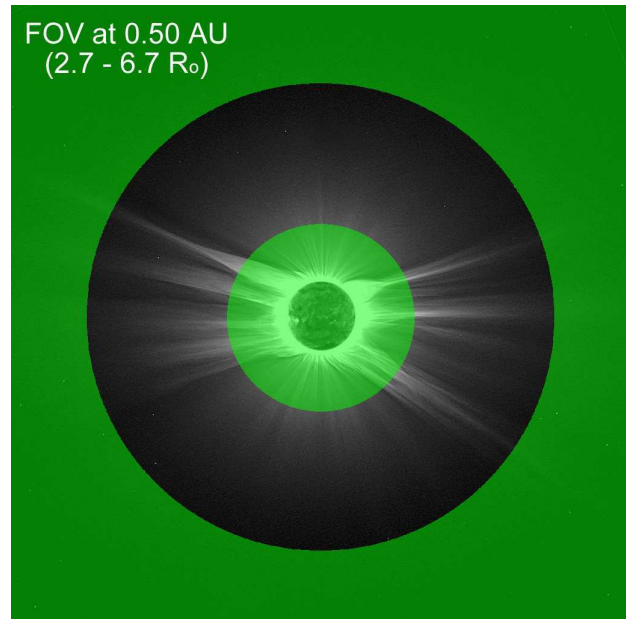
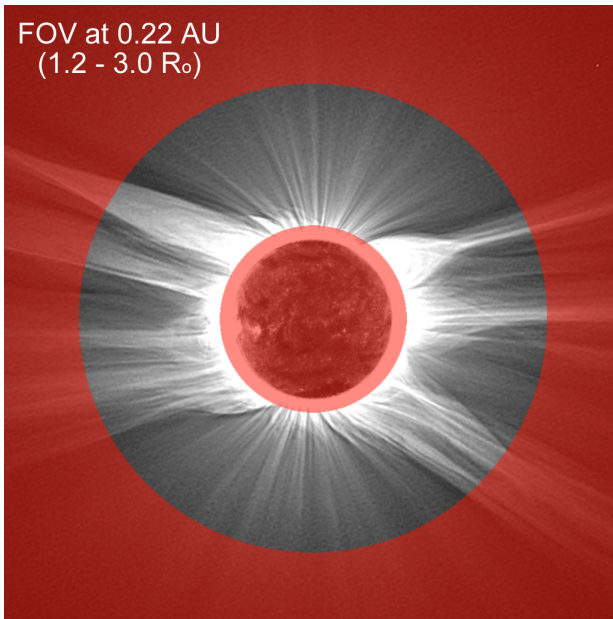


Figure 1: Left: COR field-of-view at 0.22 AU: beginning of mission perihelion (1.2-3 R_{\odot}). Right: COR FOV at 0.5 AU (2.7-6.7 R_{\odot}). Nominal observations start below this distance

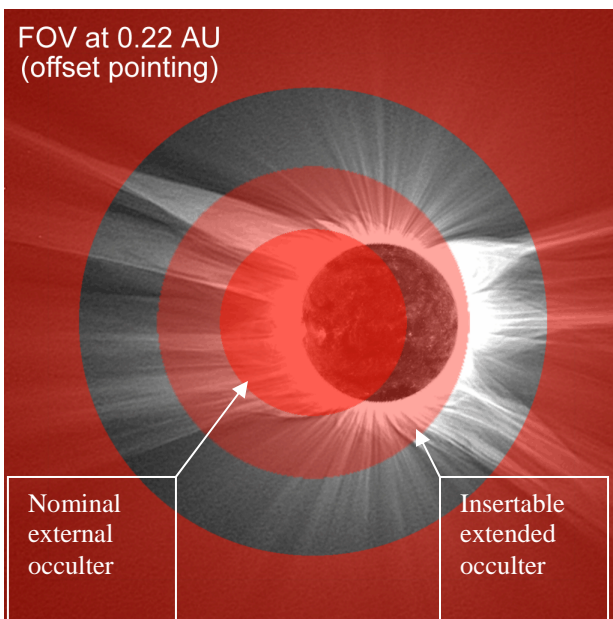


Figure 2: COR FOV during S/C offset pointing.

S/C offset pointing: COR will be capable to continue coronal observations during the S/C offset pointing, up to $\pm 1^{\circ}$, thanks to the insertion of the extended external occulter (Figure 2).

Multi-wavelength efficiencies: The optical coatings of the COR mirrors are SiC/Mg multilayers with a cap-layer capable of reflecting, in addition to the EUV (30 nm), also the UV (122 nm) and visible-light (500-600 nm) radiation. Figure 3 (at the left) shows the reflectivity of these coatings in the three wavelengths bands of COR.

COR Effective Area: The effective areas in the three COR channels, calculated by taking into account the vignetting function, the coatings, filters and detector efficiencies are shown in Figure 3 (right).

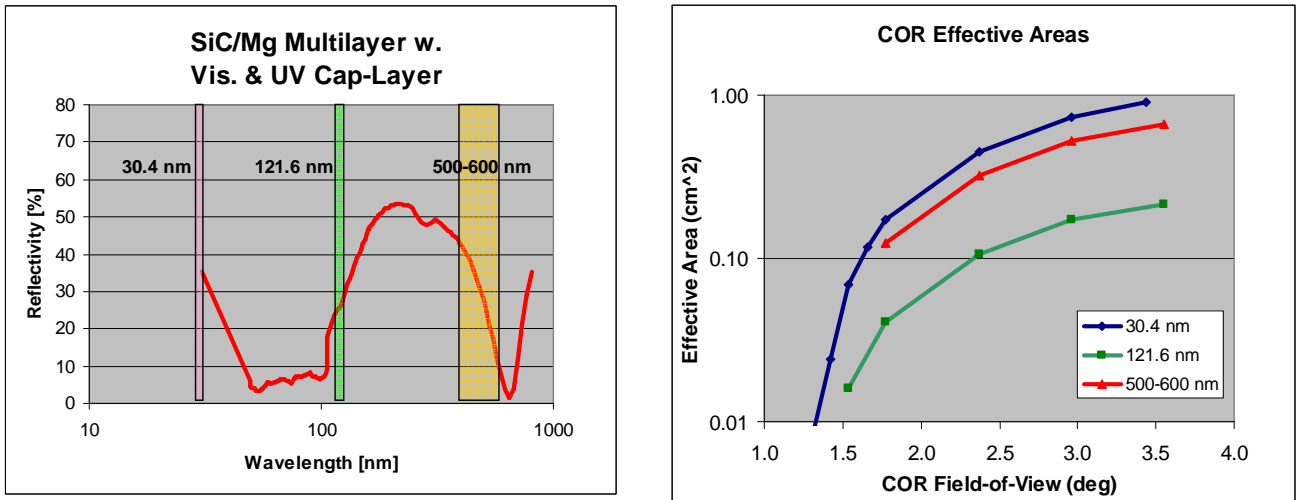


Figure 3: Left: Reflectivity of the SiC/Mg EUV multilayer with cap-layer. Right: Effective area in the 3 COR channels.

3.1.2 Expected Countrates

The COR countrates are estimated from the coronal radiances values of the K-corona polarized brightness (pB) and HI Ly- α , obtained at solar minimum with SOHO LASCO and UVCS. Whilst the HeII Ly- α countrates are derived from modelled radiances (Figure 4 and 5).

For K-corona PB images, the statistics required for achieving 1% accuracy is at least 10^4 counts. For UV /EUV images the accuracy required is 10% that is at least 10^2 counts.

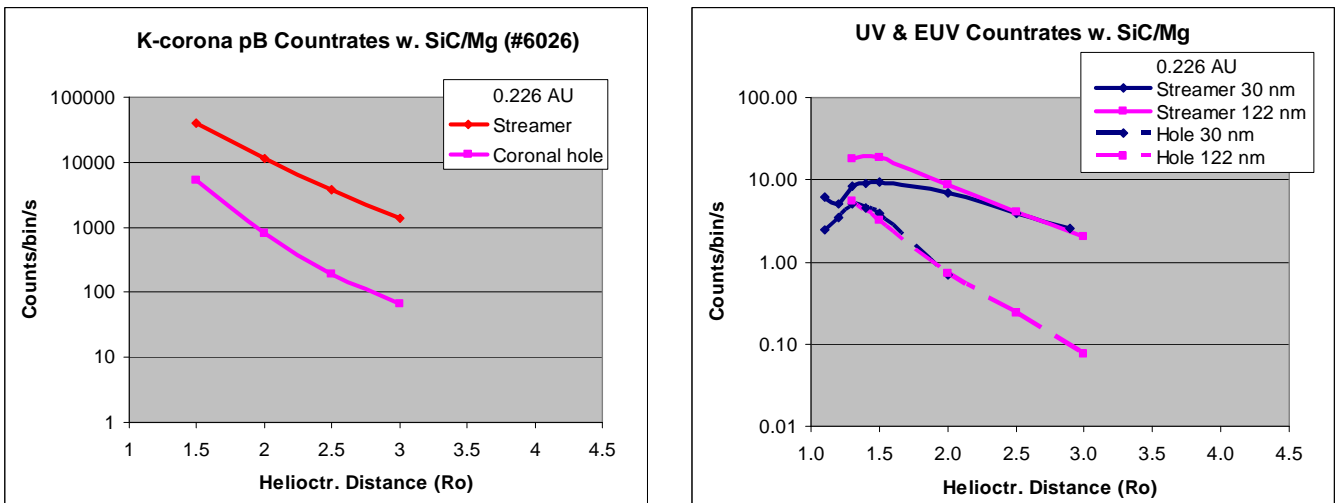


Figure 4 Count-rates for observations from 0.22 AU, perihelion at the beginning of mission. Left: Polarized visible-light K-corona. Right: HI 122 nm and HeII 30 nm coronal emission.

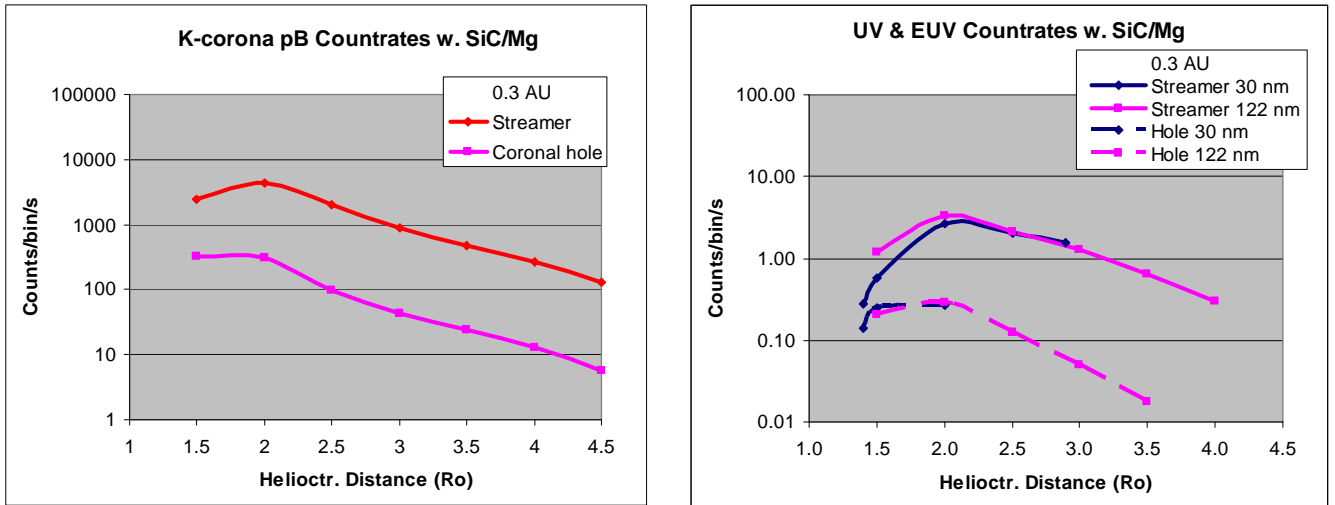


Figure 5 Count-rates for observations from 0.3 AU, perihelion at the end of nominal mission. Left: Polarized visible-light K-corona. Right: HI 122 nm and HeII 30 nm coronal emission.

3.2 EUS Extreme UV Spectrometer

The EUS instrument element is a spectrometer with three EUV spectral channels. The bands are defined in Table 2.

ID	Boundaries (nm)	Wavelength Pixel Scale (1 st order)	Spatial Pixel Scale
A [“O VI” band]	96.8 – 109.0	6 pm (18. km/s @ 100 nm)	1.2”
B [“Ly- α ” band]	116.2 – 126.6	5 pm (13. km/s @ 120 nm)	1.1”
C [“Ne VIII” band]	151.6 – 158.4	3.2 pm (6.2 km/s @ 155 nm)	1.0”

Table 2: Wavelength ranges and pixel spacing for the three bands of the EUS spectrograph.

The main solar lines in these bands are shown in Figure 6, along with a representative synthetic spectrum (computed with CHIANTI V. 5 of an “average” active region).

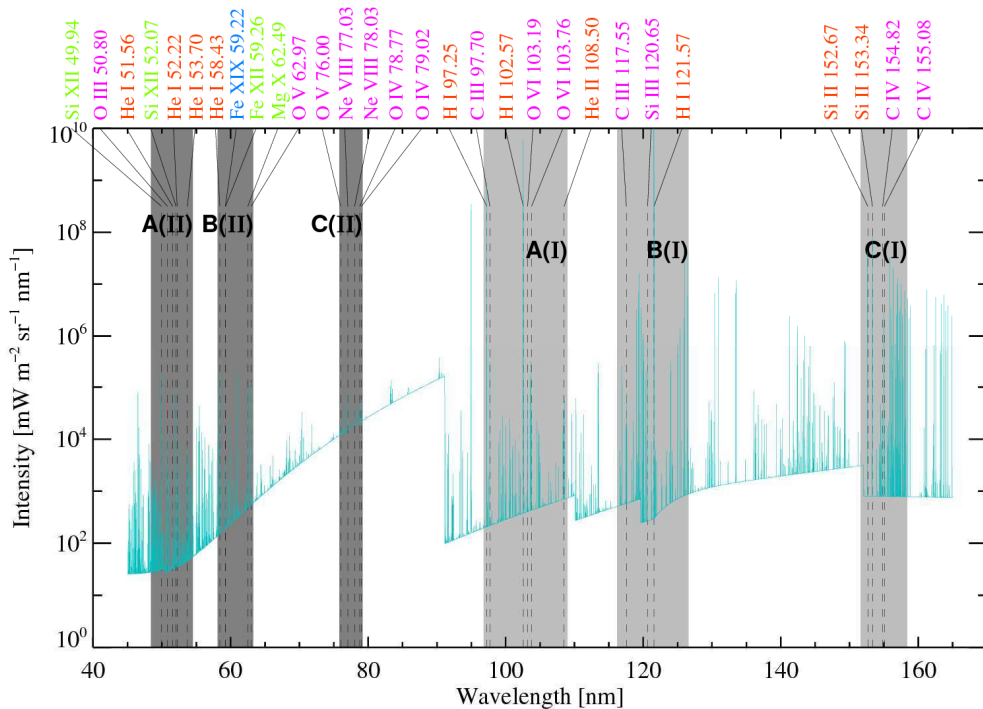


Figure 6: Wavelengths bands accessed by METIS EUS

3.2.1 Instrument Observational Parameters and Sensitivities

Wavelength Coverage of the EUS Channels: **Channel A:** the most important lines are the He II 108.5 nm, C III 97.7 nm and Fe XVIII 97.4 nm. **Channel B,** includes H I Ly- α , the C III 117.6 nm multiplet, that with the C III 97.7 nm line in band A, provides a density diagnostics in the range from 10^8 to 10^{10} cm^{-3} , a doublet, 77.0, 78.0 nm the O V multiplet at 63.0, 76.0 nm sensitive to density going from 10^{10} to 10^{12} cm^{-3} .

Temperature Coverage: The distribution in formation temperature of the strongest and/or most interesting lines in these ranges is shown in the 7. One of the main points is that the temperature range $\log T = 5.5 - 6.0$ is covered only by the Ne VIII doublet. Since that is an important range in the study of the atmosphere of coronal holes, and thus of the physics of the acceleration of the fast solar wind, the inclusion of band C in the instrument set-up is of paramount importance for that science objective.

Grating blaze angle: The grating profile is assumed to be a saw-tooth one with blaze angle equal to 15° . Although the grating diffraction efficiency, calculated at the different wavelengths and different diffracted orders, is more than 90%, the actual peak value is assumed to be 50%, since this value is within the present capabilities of grating providers. The choice of the 15° blaze angle is mainly driven by the possibility of spectroscopic observations in the outer corona of the He II at 30.4 nm line, at the 5th diffracted order, with the SOCS element, which opens the doors to novel science.

Optical and detectors differential coatings: The baseline coating for the EUS optics is B_4C , for its high efficiency for wavelengths below 55 nm. The detector photocathode is selected to be potassium bromide (KBr), with high quantum efficiency in the whole EUV region and its long-term stability. The visibility of 2nd and 3rd order spectral lines is definitely compromised unless the stronger 1st order contribution is reduced at the detector stage, as already shown by SOHO-SUMER observations. Therefore differently coated (bare or KBr) areas are adopted on the detectors for channels B and C. Channel A, on the other hand, has a uniform KBr coating.

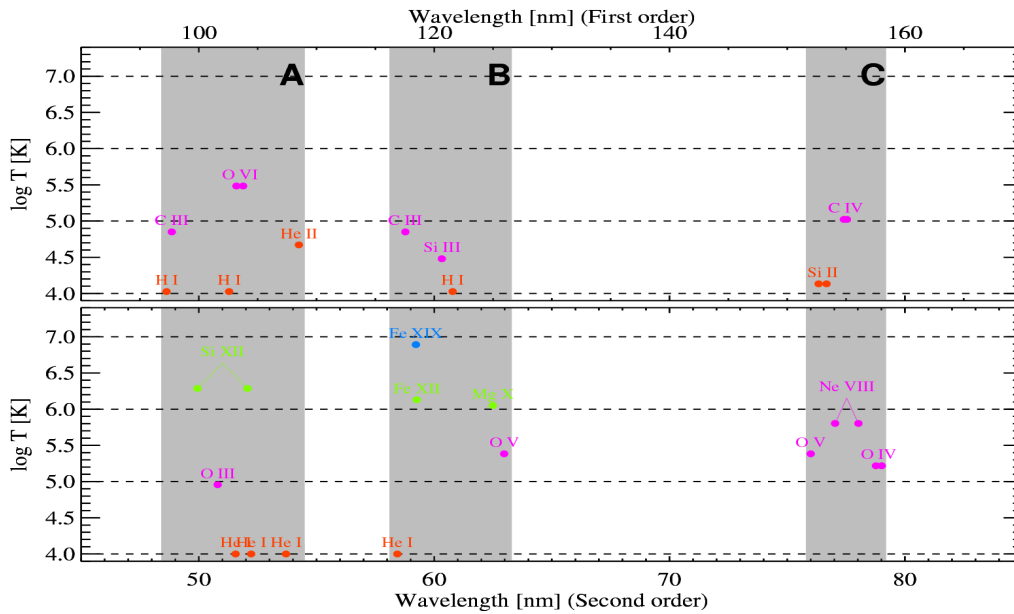


Figure 7: Formation temperatures of the ions whose lines are observed in the EUS channels. Color coding for line temperatures is: red for "chromospheric" lines; orange "transition region", green "coronal" and blue "flare".

3.2.2 Expected Countrates

On the basis of the range of intensity variability of most lines in different solar conditions, the range expected when considering near-disk and off limb measurements, and the fact that the variability in spatial observations resolved at unprecedented resolution (i.e., 160 km) is unknown due to an unknown filling factor, we assume a dynamical range of 10^3 . This is covered by changing the operational regime of the detectors that can work both in analog and photon counting mode. The expected Quiet Sun countrate across the detector of Channel B is shown as an example in Figure 8.

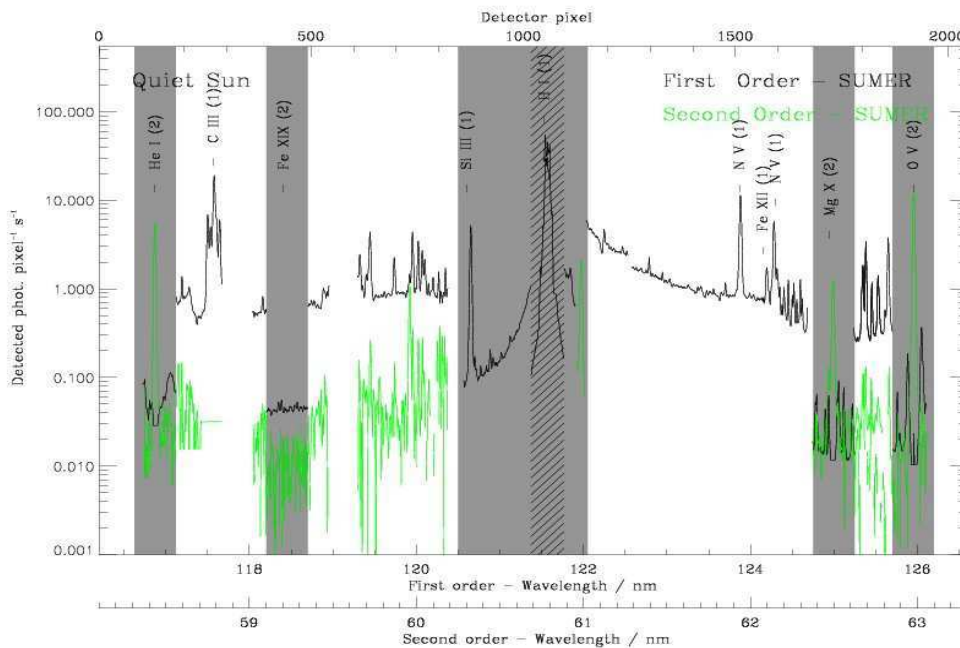


Figure 8: Simulated Quiet Sun spectral count rates in Band B. First order spectrum is shown in black; second order spectrum in green. Bare detector areas are shown as grey bands. The shaded band centred at 121.6 nm is the Ly- α attenuator for reducing the intense flux of this line.

3.3 SOCS: Solar Orbiter Coronal Spectrometer

The Solar Orbiter Coronal Spectrometer (SOCS) element is comprised of an insertable, externally-occulted telescope mirror that feeds the EUS spectrometer through multiple slits. For coronal observations, SOCS uses the same 3 spectral channels of EUS. Table 3 summarizes the coronal spectral lines covered by the 3 channels and the solar features and events that are observables with such lines.

Element	Wavelength [nm]	Ion	Quiescent Streamer	Active Streamer	CME
Channel A OVI	95.01	Si IX			X
	97.25	HI Ly γ	X	X	X
	97.49	Fe XVIII			X
	97.70	C III			X
	102.57	HI Ly β	X	X	X
	103.19	O VI	X	X	X
Channel B HI Ly α	103.76	O VI	X	X	X
	119.62	S X	X	X	
	120.65	Si III			X
	121.57	HI Ly α	X	X	X
	121.83	O V			X
	123.88	N V	X	X	X
	124.20	Fe XII	X	X	
	124.28	N V			X
Channel C HeII Ly α	130.33	Si III			X
	134.94	Fe XII		X	
	30.33	Si XI			
	30.38	He II			

Table 3 Spectral coverage of the three SOCS channels

3.3.1 SOCS Instrument Observational Parameters and Sensitivities

SOCS FOV - The multislit define four instantaneous FOVs at different angular distances from the solar West limb. The spectra from each slit are used to obtain 1-D, monochromatic images tangential to the limb, at different heliocentric heights. A full 2-D image is then reconstructed by interpolating the 4 simultaneous 1-D images. Figure 9 shows the FOV covered by the multislit at 0.22 AU and 0.38 AU. Table 4 gives the slits angular and heliocentric positions and Table 5 the optical performance of SOCS.

Slit ID	Angular Position [deg]	Heights @ 0.225 AU [Ro]	Heights @ 0.3 AU [Ro]	Heights @ 0.378 AU [Ro]
1	2.000	1.69	2.25	2.84
2	2.310	1.95	2.60	3.28
3	2.705	2.28	3.05	3.84
4	3.100	2.62	3.49	4.40

Table 4: SOCS's slits angular and heliocentric positions

Channel	Spectral plate scale [pm/pixel]	Spectral resolution [pixel]	Spectral resolution $\delta\lambda$ [nm]
A - OVI	5.96	3	0.0179
B - LY- α	5.08	4	0.0203
C - HeII (5 th order)	0.66	8	0.005

Table 5: SOCS's spectral resolution

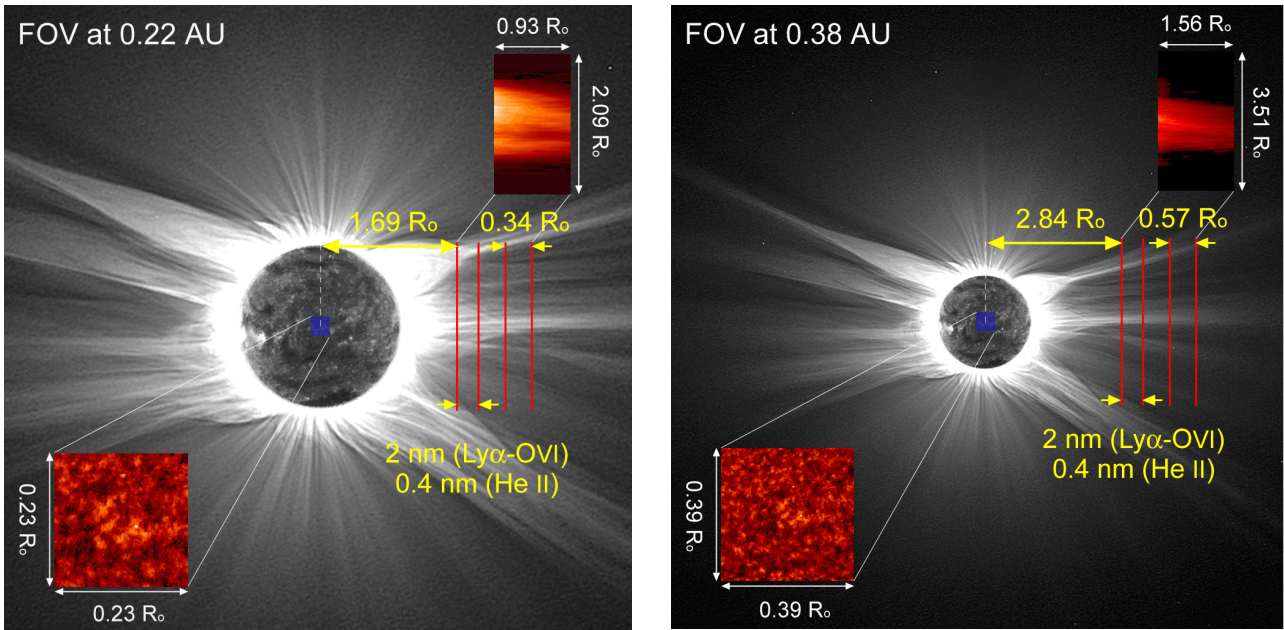


Figure 9: The SOCS's multislit defines four instantaneous FOVs at different angular distances from the solar West limb. Left: physical FOV covered by the multislit at 0.22 AU. Right: the same at 0.38 AU. The upper right insets show the full 2-D images reconstructed by interpolating the four simultaneous 1-D images. The lower left insets show disk images obtained from EUS (17-arcmin)² rasters.

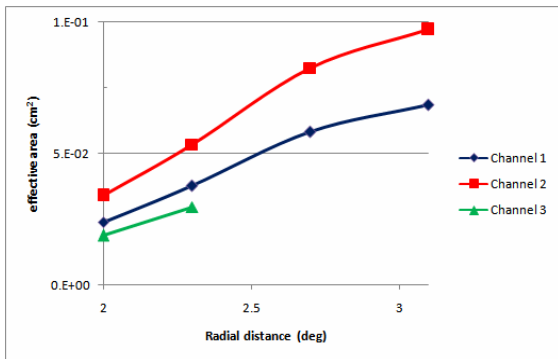


Figure 10 Effective areas of the 3 SOCS channels for each of the 4 slits (in the HeII channel only the images of 2 slits fall on the detector C).

Effective Areas and Coronal Spectra: Figure 10 shows the effective areas of the 3 SOCS channels.

The UV spectra in the wavelength range from 95 to 112 nm and 113 to 135 nm obtained with UVCS streamer data at solar minimum are used to simulate the SOCS observations. The composite UV spectrum reconstructed by superposing the UVCS spectral data obtained at the heights observed by the SOCS multislit, from a distance of 0.3 AU, is shown in Figure 11 and 12, for the OVI and HI Ly- α channels, respectively.

3.3.2 Expected countrates

The countrates expected in the SOCS HI and He II Ly α channels will be given as examples.

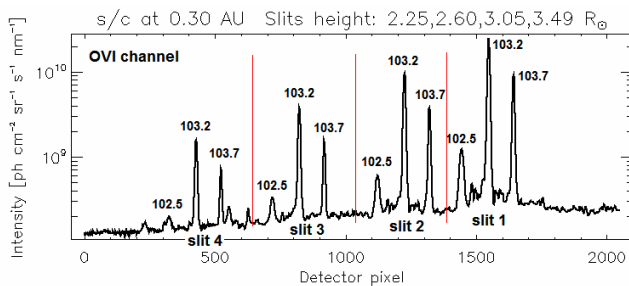


Figure 11: SOCS OVI detector simulated composite spectrum at 0.3 AU

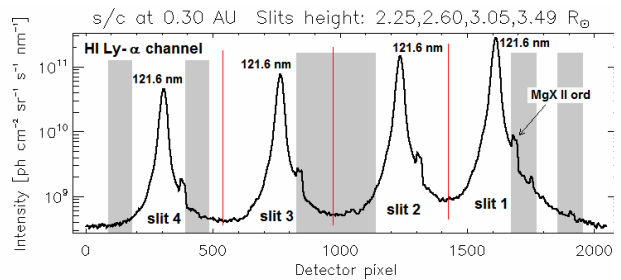


Figure 12: SOCS LYA detector spectrum at 0.3 AU, the "bare" detector regions are highlighted in gray.

Channel B – HI Ly α : Figure 13 shows the countrates as a function of pixel position on detector B, with the spatial binning along the slit of 60 arcsec (15 pxls) and a 0.025 nm spectral binning (4 pixel). Figure 14 plots the total counts for the integrated HI Ly- α 121.6 nm line, as a function of dwell time. This plot demonstrates that a spectral HI Ly- α 121.6 nm profile of 10^3 counts can be accumulated in about tens of seconds.

Channel C – HeII Ly α : Figure 15 shows the countrates as a function of pixel position on detector C, with spatial binning along the slit of 60 arcsec (15 pxls) and a 7 pixel, 0.005 nm spectral binning. Figure 16 shows the plots of the total counts, integrated over the spectral HeII Ly α 30.4 nm line (log scale), as a function of dwell time. This plot demonstrates that a HeII Lyman- α 30.4 nm line intensity of 10^3 counts is accumulated with dwell times of the order of tens of minutes. **Note that the spectral dispersion of SOCS Channel C is able to separate the HeII 30.38 nm from the SiXI 30.33 nm line. This capability is important for assessing the possible contribution of the SiXI to the narrow bandpass (1 nm) of the HeII Channel of COR.**

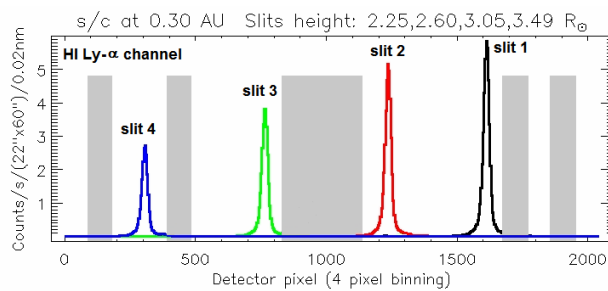


Figure 13: Ly α detector expected countrate over 4 pxl (0.024 nm) spectral bin, vs spectral pxl number at 0.3 AU.

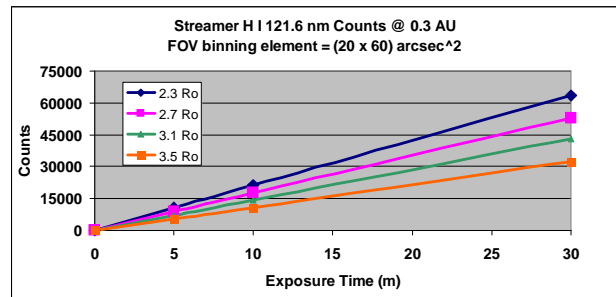


Figure 14: HI Ly α countrate integrated across the spectral line at 0.3 AU, versus dwell time.

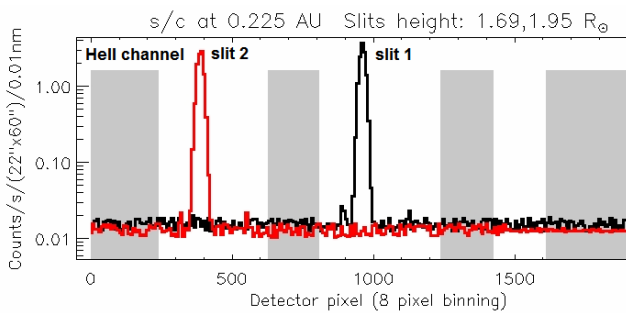


Figure 15: HeII detector expected countrate over 7 pxl (0.005 nm) spectral bin, vs spectral pxl number at 0.3 AU.

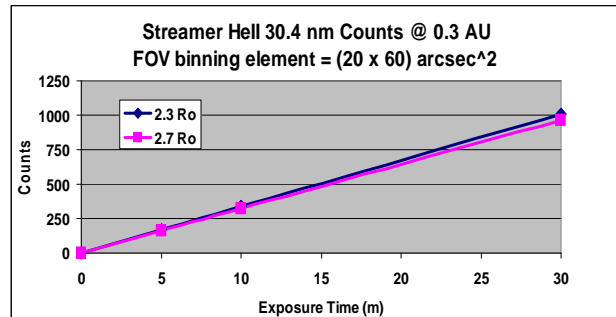


Figure 16: HeII 30.4 nm countrate integrated across the spectral line at 0.3 AU, versus dwell time.

3.4 Summary of the METIS Elements performances

Table 6 summarizes for each element of METIS, the observational drivers, observational requirements, observing modes and data products.

Table 6: METIS Elements Performance Summary

Element	Observational Drivers	Observational Requirements					Observing Mode	Data Product
		Channel	Spatial Res.	FOV	Spectr. Res.	Cadence & Exp. Time		
COR	Simultaneous UV, EUV & Visible images of full corona. Density maps Ne, N _H , N _{He, m} He absolute abundance. Outflow velocity maps of H, He+.	Visible-light 500-600 nm	13" Equiv. to 2" @1 AU at 0.22 AU	1.8-3.5 Ro @0.22 AU	100 nm	@0.22 AU 1 min. (cad) (pB = 4 frames) 10 sec (exp.)	High cadence Synoptic (during Nominal Observing Mode)	pB Images Monochromatic He II images at 30.4 nm and HI images at 121.6 nm
		UV 122 nm EUV 30 nm		1.2-3.5 Ro @0.22 AU	$\Delta\lambda/\lambda = 10$ (1 nm)	UV (20 min cad, 1min, exp), EUV (1 hr, 2 min)		
EUS	Chromospheric, TR & coronal ions temperature, density, and l.o.s. outflow velocity (>3 km/s). Ions velocity distribution Elemental composition for FIP effect assessment Reconnection signatures Waves and turbulence signatures	96.8-109 nm OVI doublet FeXXIII, FeXVIII, SiXII, OVI	1" (on disk) Equiv. to 0.14" @1 AU at 0.22 AU	Inst. FOV 1"x 17' Rast. FOV 17'x 17'	Doppler w res. 3 km/s (1/6 sub-pixel centroiding)	Exp. Time: 5 s Single step time: 20-50s Raster Cadence: 1-3 hr	Sit & stare or raster during Nominal Obs. Mode	Spectral images of the upper chromosphere, TR and inner corona corona on disk and at the limb up to 1.4 Ro (at 0.22 AU) at the brightest lines.
		116-127 nm FeXII, MgX, OV, NV, OIV	2" (off-limb) Equiv. to 0.28" @1 AU at 0.22 AU	Inst. FOV 2"x 40' Rast. FOV 60'x 40'	2 km/s			
		152-158 nm FeXXI, NeVIII, SV, OIV, NIV			1 km/s			
SOCS	Maps of ions kinetic T in the outer corona, outflow w (>30km/s) via Doppler dimming and los Doppler velocity. Images of reconnecting regions. OVI lines width broadening (CME shocks) Outer corona images at the West limb	OVI doublet 103,2, 103.7 nm, FeXVIII, SiXII	24" -60" Equiv. to 3.5"-7.4" @1 AU at 0.22 AU	Rad: 1.7-2.7 Ro	1/e los vel. distr. 60 km/s	Exp Time: 1 min. Cad. 10 min.	Sit & stare continuously during Time-share Obs. Modes and selected periods during Nominal Obs. Modes	Spectral images of off-limb corona at the brightest lines. (Instantaneous FOV at 1.7, 1.9, 2.3, 2.6 Ro, at 0.22 AU)
		HI Ly- α 121,6 nm		Tang to limb: 2.0 Ro	50 km/s			
		HeII 30.4 nm		@ 0.22 AU	100 km/s			

4 Instrument Technical Description and Design

4.1 Functional description

4.1.1 Combined Configuration METIS

The METIS instrument is an integrated suite which constitute, from a system point of view, a single interface towards the spacecraft for thermal, mechanical, electrical and optical aspects.

This suite integrates three different elements on a single optical bench also to guarantee the needed stability in coalignment between the optical heads, that is necessary for best coordinated operations and data analysis, and between the instrument and the other Solar Orbiter payloads.

A schematic of METIS is given in Figure 17.

The METIS suite consists of three different elements, each one dedicated to a specific scientific aim:

- COR, a visible-EUV coronagraph
- EUS, an EUV disk spectrometer
- SOCS, an EUV coronal spectrometer

The three elements share the same optical bench, electronics, and S/C heat shield aperture.

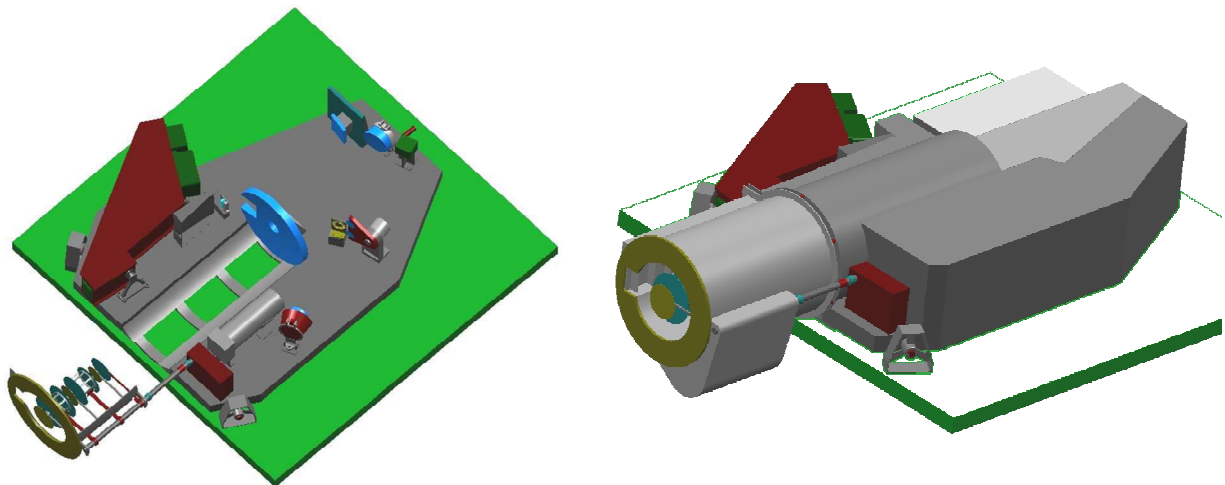


Figure 17: METIS layout: on the left the optical elements and the bench are shown; on the right, there is a view of the instrument with baffles and enclosure.

4.1.2 COR

COR is an externally occulted coronagraph designed for:

- broad-band polarization imaging of the visible K-corona;
- narrow-band imaging of the UV corona in the H I Lyman- α , 121.6 nm line;
- narrow-band imaging of the EUV corona in the He II Lyman- α , 30.4 nm line;

in an annular FOV between 1.2 and 3.0 solar radii, when the perihelion is 0.22 AU, and between 1.8 and 5.3 solar radii when at 0.3 AU.

The coronagraph critical issue of solar disk light rejection is taken care of by means of a novel optical design for a reflecting coronagraph, widely used in traditional externally occulted coronagraphs. This optical design has been thoroughly studied in the design of the SCORE coronagraph developed for the sub-orbital mission HERSCHEL.

A combination of multilayer coating of the mirrors, optimized to enhance reflectivity in the EUV He line, and of band-pass filters contribute to the capability of imaging the solar corona in three different wavelength bands by means of a single telescope. These mirrors are coated with multilayer optimized for 30.4 nm, but still have good reflectivities at 121.6 nm and in the visible.

The visible light channel and the UV and EUV channels are separated after the secondary mirror. In the UV mode, a multilayer filter reflects visible light and transmits narrow-band UV HI line. In this mode, both channels work simultaneously. In the EUV mode, the multilayer filter is replaced, by means of a two-position mechanism, by a low-pass aluminium filter that transmits the EUV HeII line. In this mode the visible light channel channel is not operative.

The visible light channel includes an achromatic polarimeter for measuring the linear polarized brightness. COR has the capability of being operative also during the spacecraft off-pointings by means of a mechanism that inserts an additional external occulter system, called off-pointing external occulter, which is large enough to prevent disk light from entering the coronagraph aperture stop. In case of off-pointing, COR FOV will not be symmetrical with respect to Sun centre.

4.1.3 EUS

The spectrometer adopts a stigmatic design in a compact package with high throughput due to the minimum number of reflections. The instrument consists of a single-element parabolic telescope which creates the image of the Sun on its focal plane. An entrance slit acts as the field stop to select the region of the Sun whose spectrum has to be acquired. A toroidal grating with variable-line-spaced grooves gives a stigmatic spectrum of each of the points along the slit height. The spectral imaging of an extended area is obtained by rastering through the rotation of the primary mirror in the direction perpendicular to the slit height. Three detectors are aligned on the spectral curve to acquire simultaneously the imaging spectra on six spectral intervals in 1st, 2nd diffracted orders. Also we expect to acquire 3rd order lines on detector 3.

The spectral intervals to be acquired are the 1516-1584 Å (1st order, detector 3), 1162-1266 Å (1st order, detector 2), 968-1090 Å (1st order, detector 1), 758-792 Å (2nd order, detector 3), 581-633 Å (2nd order, detector 2), 505-528 Å (3rd order, detector 3). The spectral resolving element corresponds to a velocity resolution of 18, 13 and 6 km/s respectively in detector 1, 2 and 3. These values can be definitely improved to a few km/s resolution by centroiding of the line profile.

Two operational modes are expected: 1) mode 1, with field-of-view of 17 arcmin (rastered) × 17 arcmin (simultaneous) and spatial resolution in the 1.0 to 1.2 arcsec range; 2) mode 2, with field-of-view of 60 arcmin (rastered) × 40 arcmin (simultaneous) and averaged spatial resolution in the 2.0 arcsec scale.

Off-limb observations up to 1.4 solar radii @0.22 AU can be done when the spacecraft is pointed off-center using the whole range of the raster mechanism in operational mode 2. The present progresses in terms of surface roughness make it possible to have a primary mirror which gives a level of stray light that is suitable for coronal observations up to the maximum rastered angle.

4.1.4 SOCS

The spectro-coronagraph acquires simultaneous spectral images of the extended corona in three different spectral bands and at four different radial distances. The instrument shares with the spectrometer the grating section and the detectors. An image of the solar corona is created on the entrance plane of the spectrometer by a low-resolution telescope that is in the shadow of the solar disk. A field stop with multiple slits is at the prime focus of the telescope's mirror. This multi-slit field stop is the entrance aperture for the spectrograph. The grating creates stigmatic spectral images of the different slits on the detectors. The number of strips in the field of view is selected with enough separation to minimize the spectral overlap of the lines dispersed by the grating.

Since the areas illuminated on the grating for on-disk and coronal observations are different, also different coatings can be adopted to select a different spectral range for the spectro-coronagraph, in particular both the coronal mirror and the grating are multilayer coated to allow observations at the HeII Ly- α @30.4 nm.

To instrument performs on the three detectors VUV/EUV spectroscopy and imaging at the OVI 103.2-103.7 nm doublet, the HI 121.6 nm and the HeII 30.4 nm. It observes simultaneous spectral images at four different radial distances (1.7, 1.9, 2.3, 2.6 solar radii @ 0.22 AU).

4.2 Hardware description

4.2.1 Optical Design

4.1.1.1 Design of the coronagraph

Light enters COR through the external occulter (EO) aperture that provides the Sun disk occultation. EO is a multiple disk system that ensures both thermal protection for the optics and better stray-light rejection. An annular sector shaped Sun-disk rejection mirror (M0) reflects back the disk light through the front aperture. The hole in M0, in the shadow of EO is the aperture stop through which the coronal light enters the telescope. The telescope consists of aspherical primary (M1) and secondary (M2) mirrors in an off-axis Gregorian mount.

The image of EO produced by M1 is blocked by a stop called internal occulter (IO). Its function is to block the solar disk light diffracted by EO. In addition, M1 forms an image of the aperture stop on the plane of M2 that is collected by a light trap behind M2, which acts as the Lyot stop. This light trap performs the final stray light rejection. The coronal radiation reflected by the secondary mirror impinges the filter wheel. The filter wheel accommodates two filters: a narrow band multilayer filter (HF) optimized to transmit the HI 121.6 nm line, and to reflect the visible light, and an aluminum low pass filter (HeF) to select the HeII 30.4 nm line. With HF, the UV HI 121.6 nm corona and the visible-light K-corona are imaged simultaneously, respectively on the UV detector and on the VL detector. With HeF, only the EUV HeII 30.4 nm is imaged on the UV detector. The optical path diagram is shown in Figure 18. A detailed description of the COR element is given in the EID-B document, part II of this proposal.

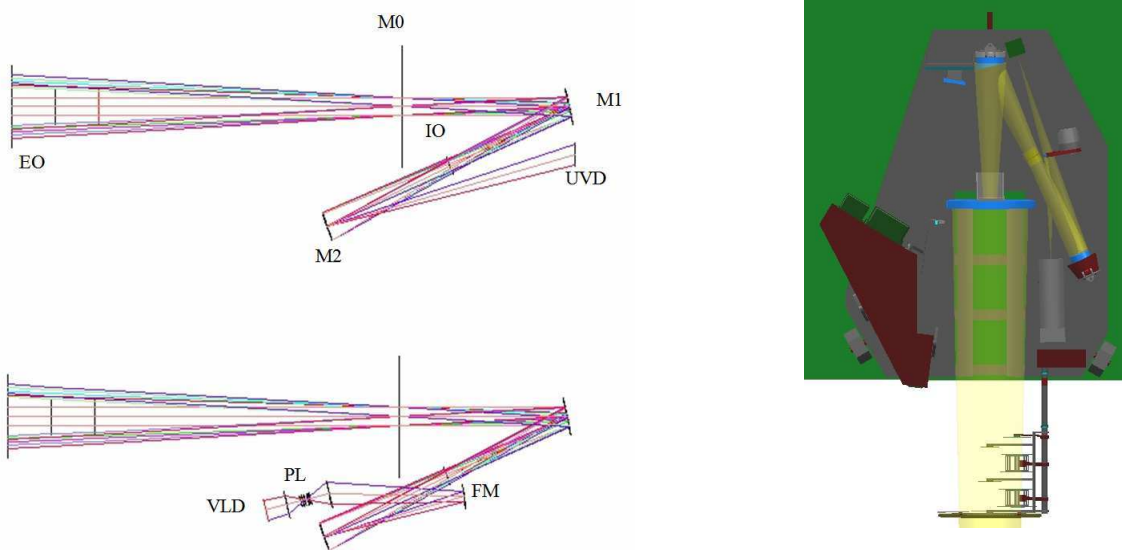


Figure 18: COR Optical path diagram..

4.1.1.2 Design of the spectrometer

The spectrometer consists of a single-element telescope, an entrance slit which acts as the field stop, a toroidal grating with variable-line-spaced grooves that gives a stigmatic spectrum of each of the points along the slit height and three detectors aligned on the focal curve of the instrument. This design has been found to provide excellent off-axis imaging in configurations with magnification higher than unity, permitting high-quality performance in compact instrument packages. Furthermore, it gives a flat focal surface in a broad spectral interval allowing the simultaneous acquisition of stigmatic images of spectral lines which are emitted by a broad range of plasma temperatures within the solar atmosphere.

The detectors are MCP-based with output on phosphor screen and APS read-out and can be operated both in analog and photon counting regimes. The MCPs will be differentially coated: 1st order lines are acquired on KBr-coated areas, 2nd and 3rd order lines on base areas, to enhance their visibility.

The primary mirror adopts a dichroic-coating design with low absorption of the solar visible and near infrared and good reflection of the VUV/EUV radiation to manage at best the huge thermal load @0.22 AU. It is coated by a thin layer of boron carbide on a quartz substrate, so the thermal load is transmitted to a great extent to the back side and dissipated through a space radiator.

The scheme of the configuration is shown in Figure 19

A detailed description of the spectrometer is given in the EID-B document, part II of this proposal.

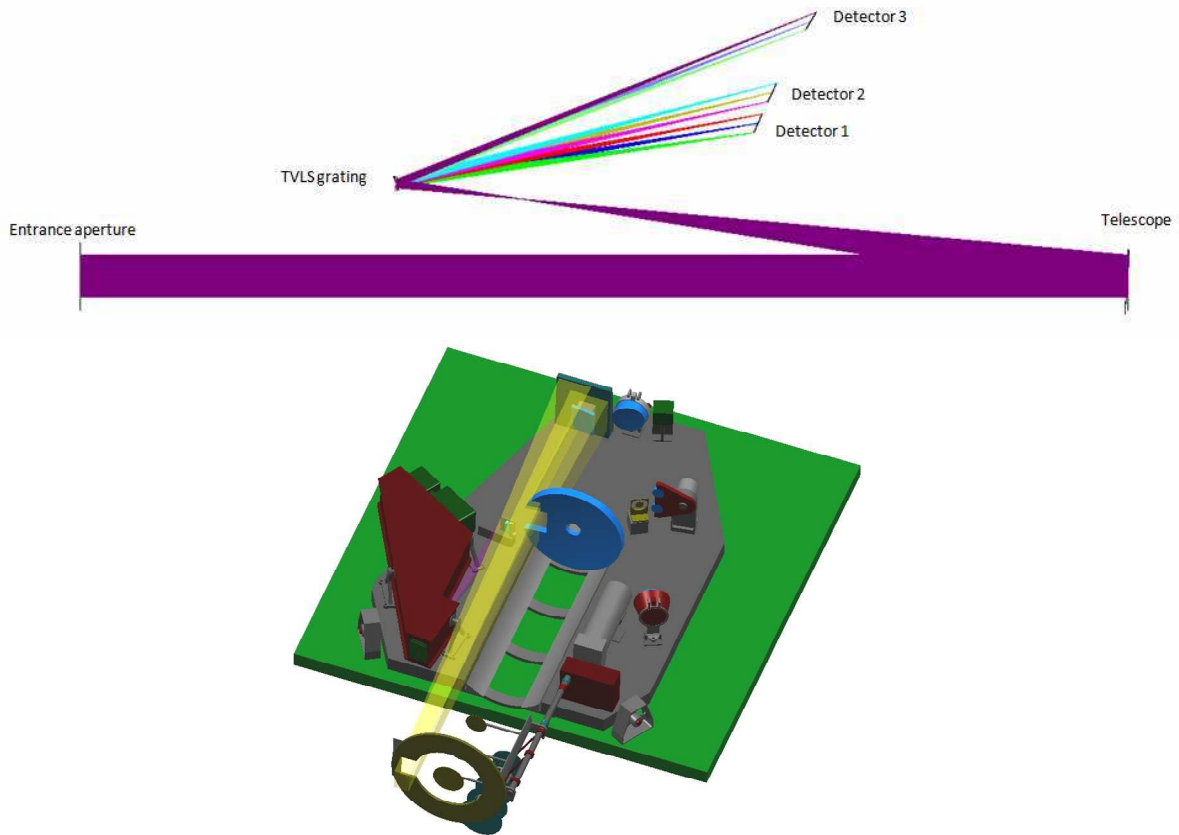


Figure 19: Scheme of the spectrometer configuration

4.1.1.3 Design of the spectro-coronagraph

The telescope that observes the corona is an off-axis parabola that is inserted in the optical path between the telescope of the spectrometer and the entrance slit plane in the shadow of the disk, as schematically shown in Figure 20. The mirror creates an image of the corona in the same focal plane of the telescope of the spectrometer. The single slit of the spectrometer is substituted by a multiple slit system with four slits that act as the field stop and let propagate toward the TVLS grating only the light coming from four distinct areas of the corona at different radial distances. The light coming from the multiple slits hits the grating in a lateral area distinct from the portion of the grating used for the on-disk observations and is then focused on the detectors.

Since the areas illuminated on the grating for on-disk and coronal observations are different, also different coatings can be adopted to select a different spectral range for the spectro-coronagraph, in particular both the coronal mirror and the grating are multilayer coated to allow observations at the HeII line @30.4 nm as 5th diffracted order in detector 3. Since the multilayer coating has rather good reflectivity also for wavelength above 100 nm, also spectral observations of OVI 103.2-103.7 nm and HI 121.6 nm at 1st diffracted order are acquired on detectors 1 and 2.

A detailed description of the spectrometer is given in the EID-B document, part II of this proposal.

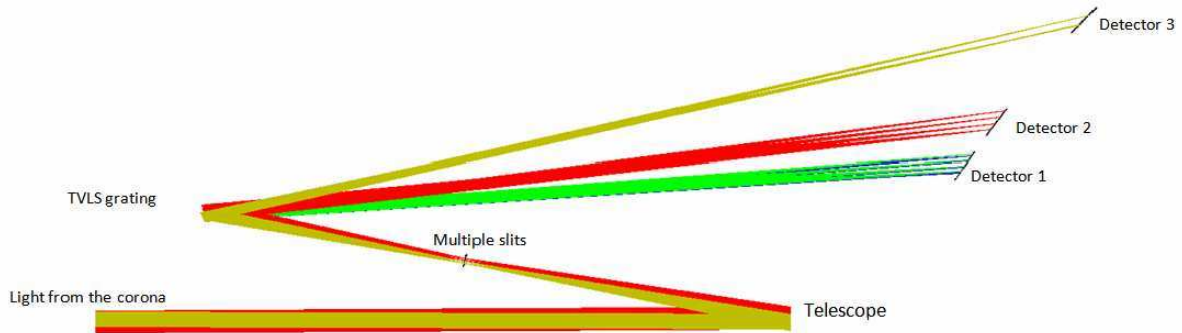


Figure 20: Scheme of the spectro-coronagraph configuration

4.2.2 Thermo Mechanical Design

The coronagraph (COR), disk spectrometer (EUS) coronal spectrometer (SOCS) forming the METIS instrument are installed on a common optical bench and share the same aperture in the satellite heat shield (Figure 4.2.2-1). The external occulter mask is supported by the external optical baffle, made in Carbon-Carbon composite (CTE = 0.2 $\mu\text{m}/\text{m}/^\circ\text{C}$, thermal conductivity = 34 $\text{W}/\text{m}/^\circ\text{C}$), through a set of thermal washers providing a first thermal cut. The external optical baffle crosses the whole heat shield and the S/C front panel, and its length can be adapted to the thickness of the S/C heat shield. Preferably, the external optical baffle should not be surrounded by an additional thermal baffle, but just by a frame (spacecraft provided) supporting the various layers of the heat shield, avoiding the direct physical contact between the shield and the baffle, but letting the optical baffle sides free to radiate the heat in the gaps between the layers of the heat shield. On top of the front shield, the frame shall overlap by about 1 cm the external occulter mask (so to cover the gap between the optical baffle and the front shield) but again without a physical contact.

On the optical bench, an internal optical baffle surrounds the sun disk and corona light beam till the sun-light rejection mirror M0. This internal baffle is inserted in a cut-out of the optical bench and fixed to the bench in eight points through two longitudinal ribs. The external optical baffle is connected to the internal baffle through an interface frame and the interposition of thermal washers to cut the heat flux towards the bench. The whole optical baffle (external + internal) is sized so to avoid direct impingement of the internal walls by the sun disk light even during $\pm 1.25^\circ$ off-pointing of the satellite from the sun center.

The three disks forming the fixed external occulter are connected one by one to a support frame (joined to the external optical baffle) by means of titanium rods (CTE = 9.2 $\mu\text{m}/\text{m}/^\circ\text{C}$ at 250 $^\circ\text{C}$, thermal conductivity = 16.4 $\text{W}/\text{m}/^\circ\text{C}$), with interposition of thermal washers. The five disks forming the removable occulter are connected by means of three titanium rods (the four outer disks are connected two by two) to a hollow shaft made in titanium and linked to the motor installed on the optical bench (a 60 $^\circ$ rotation must be applied to the shaft for moving the occulter disks from the parking position to the operative position, interleaved with the fixed disks). A thermal breaker made of ceramic material is introduced along the shaft to prevent the heat propagation towards the bench.

The optical bench is a 40 mm thick sandwich panel with CFRP skins and CFRP honeycomb. Titanium inserts are embedded in the honeycomb in correspondence of the mounts of the items installed on its surface. The SOCS elements (entrance slit, grating, detectors, shared also with the EUS) are grouped in a separate box, installed on the bench by means of three bipods. The SOCS primary mirror, as well as all the other elements of the EUS and COR (mirrors, detectors, filters, mechanisms, internal baffles) are instead directly mounted on the optical bench.

The optical bench is interfaced with the satellite by means of three “pseudo-kinematics mounts” providing a quasi-isostatic support, designed to carry the launch loads and to minimize at the same time the transfer to the bench of stresses originated by deformations of the spacecraft structure.

The hottest elements installed on the optical bench (M0, EUS heat absorber) are cooled by conduction, using thermal links (flexible straps + heat pipes) to external radiators. The heat pipes (S/C provided), should give the required I/F heat transfer capability, while the flexible connection (instrument provided) are dimensioned to discharge heat at the thermal interface point (heat pipe) with the lowest mechanical restraints.

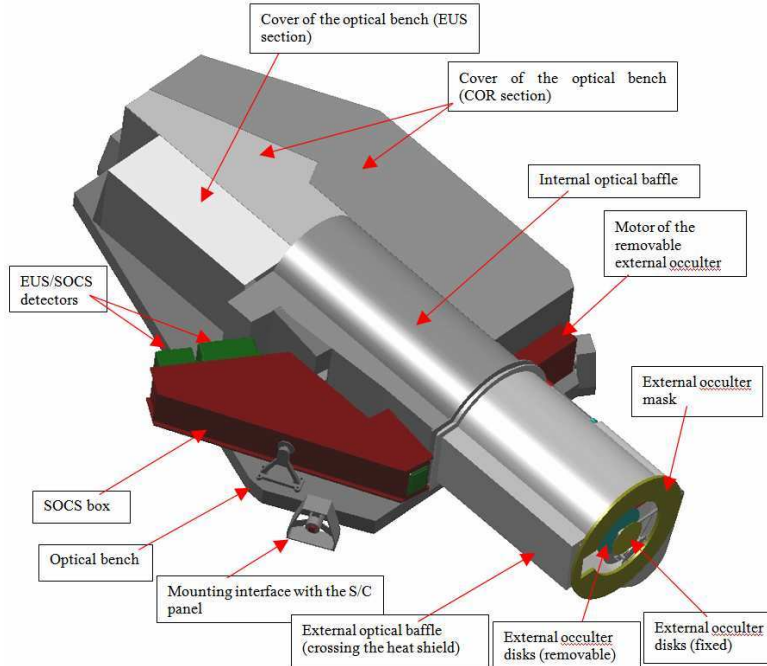


Figure 21: Configuration of the METIS instrument

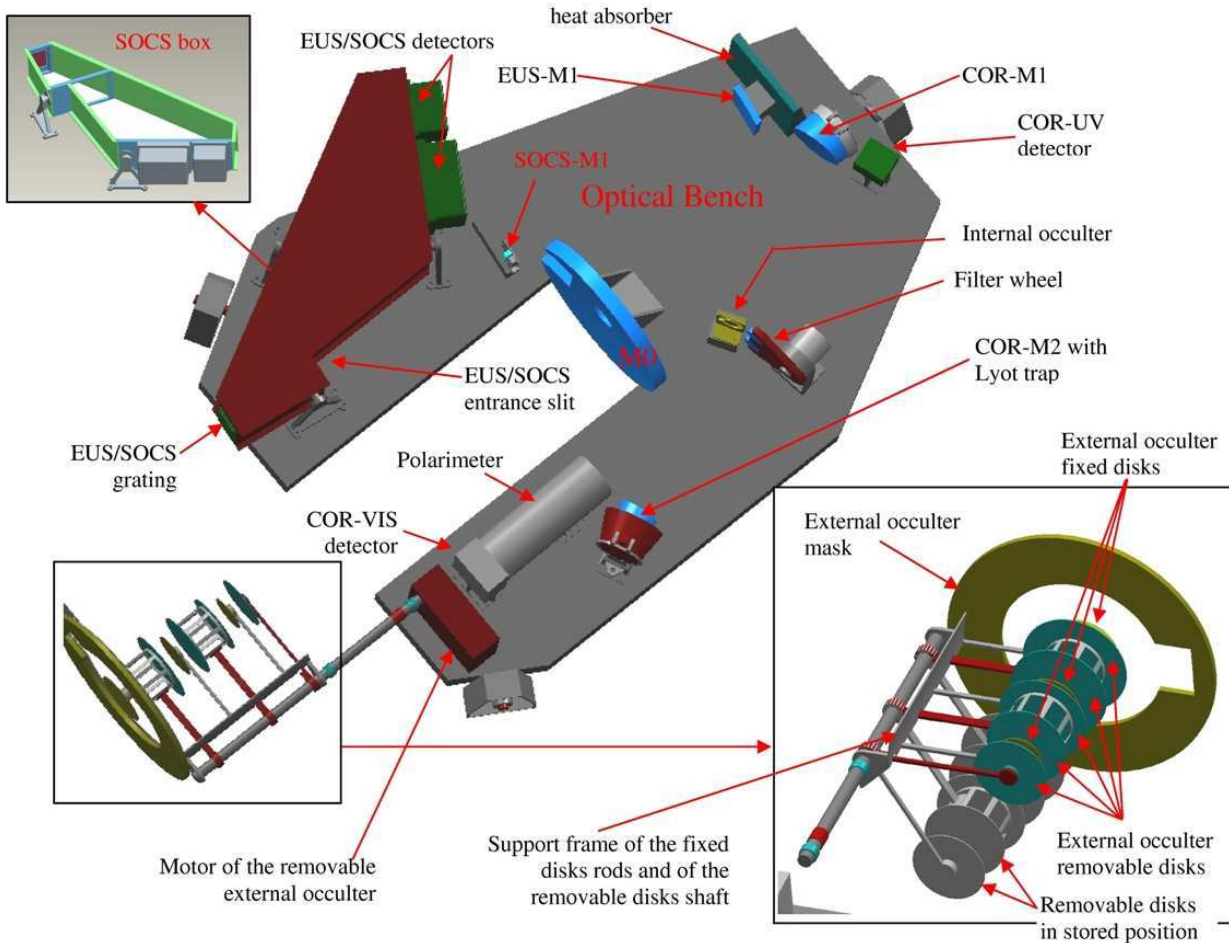


Figure 22: Configuration with optical baffles removed and detail of the external occulter

4.2.3 Mechanisms

METIS has totally 6 mechanisms.

The COR mechanisms are:

1. Extended external occulter insertion
This is a precision two-position mechanism to insert the extended external occulter without mechanically interfering with the fixed external occulter
2. Filter exchange
This is a precision two-position mechanism, that accommodates the multilayer filter and the aluminum low-pass filter, to switch from Hydrogen-visible observation mode to Helium observation mode.
3. Internal occulter alignment (during commissioning phase only)
This mechanism is necessary to adjust during the commissioning phase the position of the internal occulter to compensate for external occulter misalignment and S/C off-pointing. This mechanism is designed to adjust the internal occulter position along the axes perpendicular to the local optical axis.

The EUS mechanisms are:

4. Primary mirror scan mechanism
This is a precision mechanism that rotates the disk-spectrometer telescope mirror around a vertical axis passing through its centre to perform the rastering over an extended region. The minimum rastering step is 1 arcsec and the rastering interval ± 30 arcsec.
5. Coronal telescope insertion mechanism
This mechanism is used to insert the coronal telescope that is used to look at the corona (i.e., placed in the shadow of the disk) in the optical path through a linear displacement.
6. Slit covering mechanism
This mechanism is used to insert a mask to cover one or four slits alternatively through a linear displacement. The single slit is used for the on-disk observations, the multiple-slit system for the spectro-coronagraphy.

4.2.4 Detectors and Front-End Electronics

4.1.1.4 COR detectors

The COR visible detector will be a custom developed Active Pixel Sensor (APS).. The sensor has a format of $2k \times 2k$ with pixel size of $25 \mu\text{m}$. The most critical parameter with the currently available technology is the readout noise, which in the baseline has to be less than $5 e^-$. This point could be addressed with a specific 1-2 years development program. However, a readout noise of $10 e^-$, which is in the current technological capability, could be tolerable.

Due to the relatively long acquisition frame period, the APS should be operated at low temperatures (of the order of -50°C) and therefore should be equipped with a thermoelectric cooler device and a suitable radiator.

For this sensor, the ADC should be off-chip. Even if in this way the external electronics is more complex this allows more flexibility of ADC design, better radiation hardness options and less complexity of the sensor itself, allowing better performance in terms of noise.

The COR UV detector works in photon counting and is based on the same design of EUS/SOCS detectors, using the same IAPS sensor. The difference in the required pixel size ($25 \mu\text{m}$ pixel size instead of $12 \mu\text{m}$) can be overcome coupling a larger MCP intensifier (diameter $> 50 \text{mm}$) to the smaller sensor with a fiber optic taper of appropriate reduction ratio (2:1). Since the APS format is the same than the required detector format, no sub-pixel resolution with event centroiding is required, but only the event peak detection.

4.1.1.5 EUS/SOCS detectors

The spectrometer and the spectro-coronagraph use the same detectors, but in two completely different intensity regimes: in fact, since the two elements look either at the disk or at the corona, with orders of magnitude of different light intensities, the detectors have to be able to work with an extremely large dynamic range.

The baseline for the detector architecture is an Intensified Active Pixel Sensor (IAPS), since it allows operation in two different modes, photon counting and integration exposure, suitable, respectively, for low and high level of flux. The schematic of the IAPS detector is shown in Figure 23.

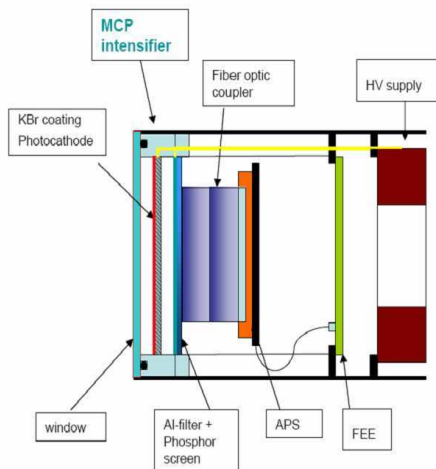


Figure 23: Schematic of the IAPS detector.

housing with a door (single shot aperture, TBC) to be opened once in orbit and when in operation during the laboratory characterization and calibration phases.

4.2.5 Electronics

The METIS electronics (called MPPU, METIS Processing & Power Unit) is the unique interface of the instrument with the Spacecraft (Power, Science Data, TM&TC). On the S/C side, the MPPU interfaces with the data handling system using a dual cold redundant Spacewire Interface for transmission of TM and reception of TC packets, and with two independent primary power lines.

On the instrument side, the MPPU interfaces with the front-end electronic (FEE) boards of the 5 APS detectors (COR-VIS, COR-UV, EUS/SOCS spectral channels 1, 2, 3), with the Thermoelectric Coolers of these detectors, the thermistors for the temperature monitoring, and with the mechanisms described in section 4.2.3. The high-level architecture of the METIS electronics is provided in Figure 24, where the MPPU links with the detectors and mechanism are shown.

The main functions of the MPPU are:

- Receive the power from regulated bus of the Spacecraft and
 - generates all the voltages needed by the various boards inside the MPPU
 - supply the FEE boards (including the high voltage needed by the Microchannel Plate - MCP - of the UV detectors);
 - drive the Thermoelectric Coolers for stabilizing the detector temperature;
 - supply all the motors of the mechanisms;
- Receive and execute the TCs coming from the S/C.
- Manage the operating modes of the COR, EUS, SOCS and control the detector temperature.
- Collect the science data from the COR, EUS, SOCS detectors FEE, store them into a Science Memory Buffer and perform a first data processing/compression.
- Collect the HK of the whole instrument (including temperatures).
- Generate the HK and Scientific Telemetry packets and transmit them to the spacecraft through a SpaceWire link using the ESA Remote Terminal Controller (RTC) or equivalent device.

The main functions of the detector FEEs (to be placed as close as possible to each detector) are:

- Filter the power supply lines needed by the detector, and in particular the high voltages used as a bias of the MCP;
- Supply clock and bias to the five APS detectors and generates all the reference needed;
- Implement hard coded read-out routines windowing/sub-windowing.
- Implement the analogue to digital conversion using one or more 12-bit (TBC) ADC.
- Interface with the MPPU using a fast serial digital connection.

MCP intensifiers can be operated both in analog and in photon counting mode by changing their operating voltage. The APS readout system is well suited for both operating modes:

- in analog mode the input image is read out by the APS directly sensing the output of the phosphor screen
- in photon counting, the APS is operated at a frame rate high enough not to have overlapping of the spots generated by each primary photon; then each frame is searched to recognise these spots, computing the x, y coordinates of their centers

A 2k×2k pixel sensor will be used.

The three SOCS detectors will use basically the same design, with differently coated area to optimize the sensitivity for each channel at the 1st diffracted order or at the higher orders.

The Front End Electronics will include the APS controller, which will provide the digital signal sequences to operate the sensor, and a digital data processing block, implementing different functions in the two, photon counting and analog, operating mode.

All the IAPS detectors (both for COR and EUS/SCOR) will be in open configuration: the intensifier will be hosted in a vacuum

The following boards are foreseen in the MPPU to implement its functions:

- two DC/DC converter boards for high voltages of the COR-UV and EUS/SOCS detectors;
- two DC/DC converter boards for MPPU and FEE board power supplies;
- two digital interface boards to manage the detector FEEs;
- one board implementing the drivers for the Thermoelectric Coolers (TEC) of the detectors;
- two boards implementing the drivers for all the mechanism;
- one board to collect the analogue HK and implement the mass memory for science data;
- one micro-processor board with the cold redundant Spacewire Interface;
- one micro-controller board;
- one motherboard (backplane).

MPPU estimated volume = 220×250×350 mm³
mass = 10.3 Kg (inclusive of 25% of margin)
power consumption = 37 W (inclusive of 25% of maturity margin)

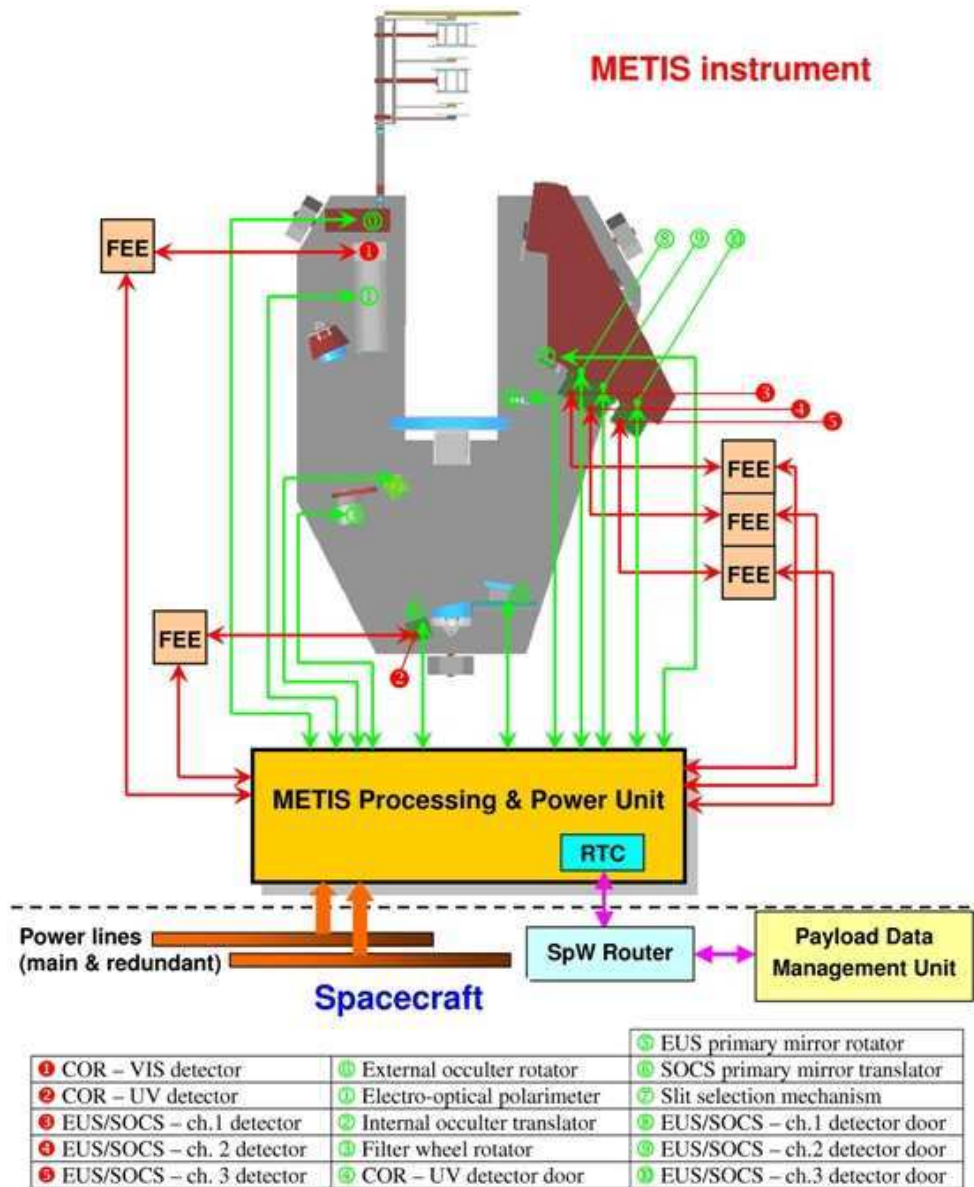


Figure 24: METIS High Level Electronic Architecture

4.3 Software description

Software architecture is based on the highest possible level of integration, in order to achieve a single interface to the spacecraft and avoid duplication of functions that are common to Instrument Front End elements. In particular, data compression is centralized for all the elements. A common communication protocol is identified for the link between the elements and the common electronics. Spacewire interface implemented within FPGA represents a viable choice, thanks to its flexibility and speed. This approach has also the advantage to make the operation of a single element easier during assembly and verification, before its integration at instrument level. Spacewire is envisaged even for communication between the main electronics and spacecraft, both for data link and for telecommand / telemetry link.

Specific features to be developed for METIS on board software can be identified in the following topics:

- Autonomous MCP protection. To increase the MCP lifetime, an internal watchdog routine or task shall be defined to verify if the incoming radiation is below a specific threshold. Passing the threshold will put the instrument in safe mode.
- S/C offset from the Sun center: The S/C will have to deliver periodically the pointing offset telemetry from the Sun Center in order to protect the COR element.

4.4 Operational modes

The functional operating modes of the METIS suite can be subdivided in

- **Off** - instrument switched off before commissioning
- **Safe/Standby** (high voltage power supply off) - if S/C off-pointing larger than $\pm 1.2^\circ$ @ 0.22 AU, emergency Sun re-acquisition, orbital manouvers
- **Calibration modes** (ground and in flight calibration)
- **Observational modes**

The observational modes defined in what follows are adopted to address the scientific objectives described in Sect. 2.

The observational modes, subdivided according to the METIS element, are reported in the following table:

METIS Element	Channel	Observational mode ID	Pointing	Observation Product
COR	Visible & UV Imaging Coronagraph	COR-SC-UV	S/C Sun Center	Simultaneous images in HI Ly α 121.6 nm and polarized visible light
COR	Extreme UV Imaging Coronagraph	COR-SC-EUV	S/C Sun Center	He II Ly α 30.4 nm monochromatic images
COR	Visible and UV Imaging Coronagraph	COR-OP-UV	S/C Off Pointing (OP)	Simultaneous images in HI Ly α 121.6 nm and polarized visible light
COR	Extreme UV Imaging Coronagraph	COR-OP-EUV	S/C OP	He II Ly α 30.4 nm monochromatic images
EUS	Disk Extreme Ultraviolet Spectrometer	EUS-D	S/C Sun Center	EUV rasters on disk (emission lines in the range 96.8-158 nm)
EUS	Off Limb Extreme Ultraviolet Spectrometer	EUS-L	S/C OP	EUV rasters on disk (emission lines in the range 96.8-158 nm)
SOCS	Near-limb Extreme Ultraviolet Spectro-Coronagraph	SOCS	[OFF when S/C OP East of Sun Center]	EUV coronal spectro-images OVI doublet, HI Ly α , He II Ly α

Table 7: METIS Observational Modes

4.5 Critical Technologies

4.1.2 Polarimeter

The COR visible-light channel comprises a liquid crystal polarimeter that electro-optically modulates the K-corona pB signal without the need of mechanically rotating the polarizing optics. Although successfully proven from the ground on March 29, 2006 during an eclipse, some development is needed to space-qualify the liquid crystals. The SCORE sub-orbital mission will demonstrate for the first time the operations of liquid crystals in space.

The use of liquid crystals has clear advantages over more classical methods of mechanical modulation by rotation of polarizing elements, since no mechanism is required, the control hardware is compact and light-weighted and the power consumption is limited.

In case of space qualification delay or unavailability of achromatic liquid crystals, a rotating half wave retarder plate followed by a fixed linear polarizer acting as analyzer will be necessary. This solution requires an additional COR mechanism to drive the retarder plate inside the optical path and the addition of a color filter in front of the polarimeter assembly.

4.1.3 Multilayers for COR and SOCS

Classical EUV multilayer structures, such as for instance Mo/Si, have the capability of reflecting at longer wavelengths in the UV and visible thanks to the protective cap layer deposited on top of the layer stack. The optical design of COR and SOCS takes advantage of this capability by combining in one set of optics three wavelength channels.

In order to extend and optimize the EUV multilayer reflectivity into long wavelengths, a technological program is being carried out for the development of multilayers with cap-layers with enhanced throughput at 103 nm and 122 nm (SOCS) or 122 nm and visible (COR). In particular, SiC/Mg multilayers with visible/UV cap-layer have been proved to give definitely higher reflectivity in the EUV. At present, this coating needs further developments for the space qualification. We will pursue all the efforts to choose the best multilayer coating which optimizes the response in the whole spectral region of interest of COR and SOCS.

The backup solution for multilayers is to adopt the well-known space-qualified Mo/Si combination with SiO₂ cap-layer.

4.1.4 IAPS Detectors for EUS/SOCS

Some testing and the space qualification are necessary to have a model of the IAPS detectors reliable for flight for EUS/SOCS. In particular, some development will be necessary to guarantee the capability of maintaining the high spatial resolution in both photon counting and analogue modes on the same detector. All the other points are rather well consolidated (such as APS, front-end electronics, remote electronics) and do not need any specific development.

However, in the worst case this detector will not be available in time, a backup solution can be easily found changing the SOCS optical design, and increasing the grating-to-focal plane distance. In fact, in this case, a larger pixel size is necessary, and consequently a larger detector, but at the same time this greatly reduces the spatial resolution criticality. In practice, an IAPS with a larger APS pixel size would allow to maintain the foreseen scientific performance of the instrument, at the minor cost of some increase of the needed mass resource.

4.6 Minimum METIS configuration

The minimum METIS configuration is the following:

- Reduction of the spectral channels of EUS/SOCS from 3 to 2 with a redefinition of the spectral bands. This reduces the number of the EUS/SOCS detectors to 2, consequently also the mass and the complexity of the electronics.
- Cut of the EUV channel of COR, that observes HeII Lyman- α line. This eliminates the filter exchange mechanism.

5 Summary of Experiment Interfaces

5.1 External Configuration Drawings

The external configuration of METIS instrument is shown in Figure 21. The main dimensions of the external envelope are provided in Figure 25. The instrument power supply and data handling electronics is contained in a box (the METIS Processing & Power Unit) having an envelope of 220×250×350 mm³.

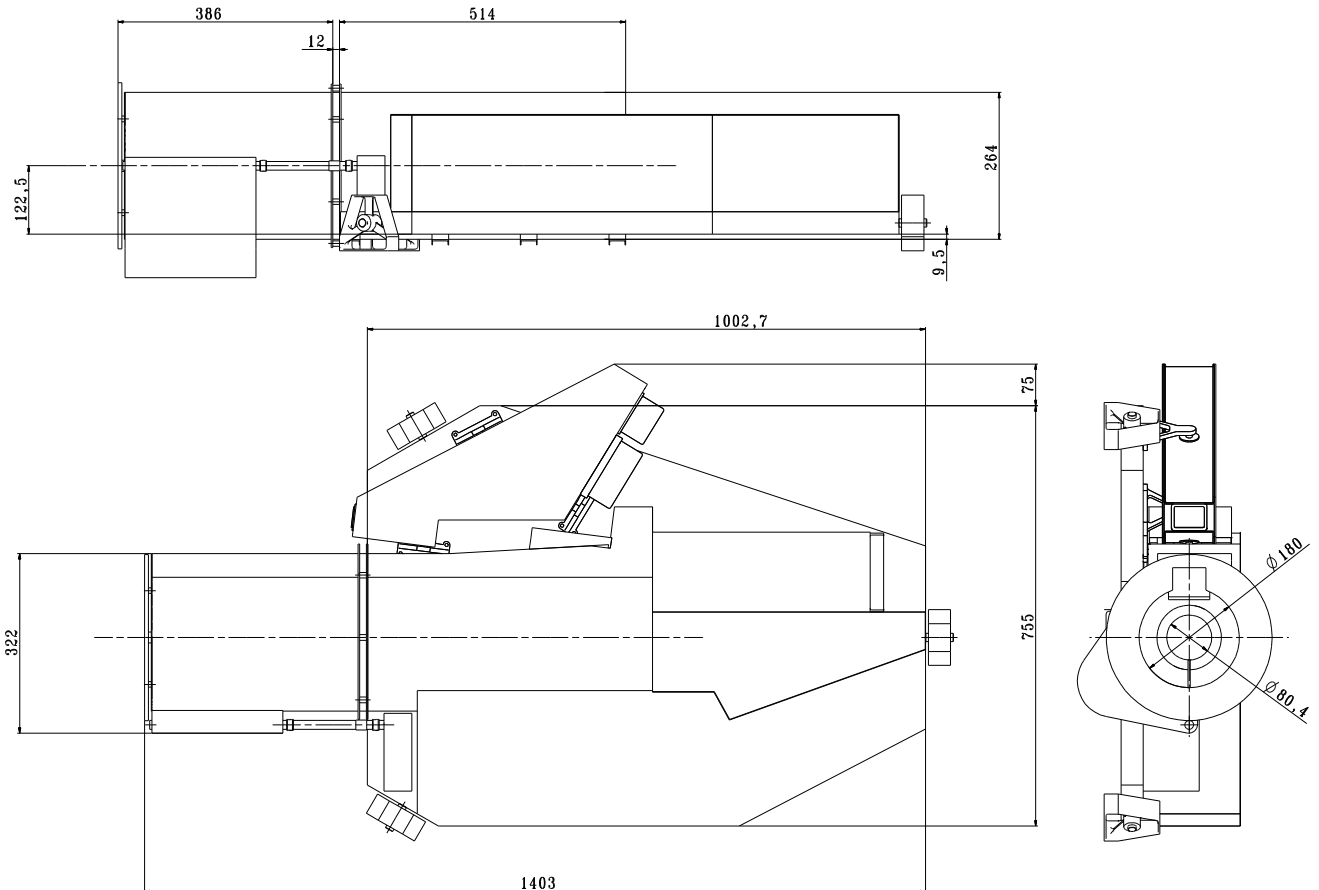


Figure 25: METIS external envelope main dimensions

5.2 Summary of METIS interfaces

Optical Bench Size	1408(*)x755x264mm
Electronic units Size	220x250x350mm ³
Instrument mass (inclusive margin):	37.0 kg
Center of Mass (excluding electronics box)	CoM _X = -0.314m, CoM _Y = -0.390m, CoM _Z = 0.116m.
Moment of Inertia:	I _{xx} = 1.0 kg·m ² , I _{yy} = 3.8 kg·m ² , I _{zz} = 4.5 kg·m ²
Power consumption (nominal, inclusive margin)	50.2 W@28 V
Average Telemetry Rate	26.8 kb/s

(*) 400mm are protruding through the sun shield

Table 8: Summary of METIS interfaces

6 Test and Calibration Plan

This section deals with the description of the activities to be carried out on ground during assembly and verification phases and in flight during commissioning, cruise and observational phases to fully characterize the instrumental response.

6.1 Testing

6.1.1 Ground/pre launch Tests

6.1.1.1 Sub-system tests

Subsystems of the METIS elements for which tests will be performed and documented are reported in Table 9.

COR	EUS	SOCS
External occulters	Telescope	TVLS grating
Heat rejection mirror	Raster mechanism	UV detectors
Telescope (including multilayer coating)	Slit mechanism	
Internal occulter mechanism	Coronal telescope mechanism	
Filters		
Filter mechanism		
Visible detector		
Polarizer system		
UV detector		

Table 9. List of METIS sub-systems for which tests will be performed.

For each subsystem, the following documents, when applicable, will be part of the FM delivery Data Package:

- General
- Functional Testing at Instrument Level
- Functional Testing at System Level
- EMC Testing
- Structural Testing
- Mechanism Testing
- Thermal Testing
- Log Book of test activities;
- Data Book on the experimental set-up
- Data Book of the characteristics of subsystem under measure

Considering the past experience of the Institutes and Industries involved in the project, most of the required equipment for the tests described in the following is already available. Many of the above tests will be provided by the manufacturer; however in some instances tests will be performed by Institutes/Industries as appropriate. All the METIS mechanism will follow a full qualification process as required and explained in detail in section 6.4.6 of EID-A.

6.1.1.2 Element tests

Each METIS element will be properly aligned and the alignment verified prior to the final element integration.

6.1.1.3 Instrument tests

METIS will be subjected to a Full Functional (Performance) Test (FFT) to demonstrate that the hardware and software meet the performance requirements within allowed tolerances, compliant with the requirements described in section 6.4.2.1 of RD1.

6.1.1.4 S/C tests

After integration on the satellite, METIS will undergo the qualification/acceptance test programme according to agreed system level requirements.

6.1.2 Cruise Tests

Presently, it is not foreseen to realize test activities during the cruise phase.

6.1.3 In orbit Tests

Possible in-orbit tests on METIS elements or sub-systems are still TBD.

6.2 Calibration

6.2.1 Ground/pre launch Calibrations

6.2.1.1 Calibration at element level

The calibration activity will provide the characterization of the spectral, geometric, radiometric and linearity properties of each assembled element. The measurements will be performed in a meaningful sub-set of operative modes, as applicable. The list of the presently foreseen calibration activities at METIS element level is shown in **Errore**.
L'origine riferimento non è stata trovata.

Element	Measurement type	Measurement subtype	Note	
COR	Geometric calibration	Point Spread Function		
		Knife Edge Function		
		Field of view		
		Focal length		
		Scale plate factor		
		Distortion		
		Vignetting		
		Flat Field		
		ILS alignment	With respect to the reference cube	
		Focus stability	Vs temperature	
		Baffle alignment		
		Stray light rejection		
		Radiometric calibration	Background	
			Spectral responsivity	
			Photometric responsivity	Absolute and relative
Linearity	Versus time and flux			
Saturation				
EUS	Geometric calibration	Point Spread Function		
		Knife Edge Function	Low priority	
		Field of view	Low priority	
		Focal length		
		Scale plate factor		
		Distortion	Low priority	
		Vignetting	Low priority	
		Flat Field	Low priority	
		ILS alignment	With respect to the reference cube	
		Focus stability	Vs temperature	
SOCS	Geometric calibration	Point Spread Function		
		Spectral resolution		
		Flat Field		
		ILS alignment	With respect to the reference cube	
		Focus stability	Vs temperature	
		Baffle alignment		
		Stray light rejection		
	Spectral calibration	Spectral resolution		
		Radiometric calibration	Background	
	Spectral responsivity			
	Linearity		Versus time and flux	
Flat field	Along the slit			
Vignetting	Along the slit			

Table 10. List of presently foreseen calibration activities at METIS element level.

Moreover additional calibration will be devoted to the functional tests of the digital electronics, as:

- Verification of the data flow
- Data compressor tests
- Operative modes evaluation.

6.2.1.2 Calibration at Instrument level

A subset of the calibration activities, mainly geometric and radiometric cross-calibration, will be performed on the integrated IFE to verify the instrument behavior prior to the delivery.

The verification of proper co-alignment among the METIS elements is required to guarantee the correlation of observations and to achieve the best scientific return from the combination of parallel and/or subsequent observations.

For the integrated suite of instruments the following activities are planned:

- Co-alignment of each element boresight direction with respect to the $+Z_{\text{Opt}}$ axis
- Cross spectral calibrations
- Radiometric cross-calibration

6.2.1.3 Calibration at System level

Co-alignment with other instruments on board Solar Orbiter is foreseen. This activity must be performed within the AIV plan of activities at S/C level.

During the integration of the science payload onto the S/C, the system will be subjected to mechanical and thermal test campaigns. It is foreseen to perform various instrument checks after each critical step, to verify the health status of the instrument.

6.2.2 Cruise Calibrations

During cruise periodic check-out are required. The long cruise phase (more than 3 years) recommends that tests of the instruments be performed: hence every 6 months a test run (TBD) should be envisaged.

6.2.3 In orbit Calibrations

The general purposes of in-flight calibration measurements are:

- to provide post-launch calibration verification with the aim to check in-flight the validity of the results obtained during ground calibration and take proper actions, if needed
- to monitor the instrumental performance and detect any changes, particularly those associated with degradation by contamination
- to establish the pointing of the instruments relative to spacecraft axes and other instruments and detect any launch induced changes

During the nominal mission, calibration run shall be implemented to verify element and instrument behavior. Internal calibration sources are presently envisaged (TBC) to perform a detector sensitivity analysis.

A calibration session will be dedicated to the alignment of the COR boresight direction towards the center of the Sun: this is a rather critical alignment, and it will be characterized by the analysis of the diffraction from the external occulter edge.

A potentially important absolute radiometric in-flight calibration could be observations of standard UV stars (TBC). These can be observed by the different elements, both in imaging and spectroscopic mode, and can provide both relative and absolute response information (although over a rather limited portion of the image/spectrum). Furthermore, stellar observations will provide pointing information and will be used to determine the point spread function of the telescopes.

7 System Level AIV

7.1 Verification Program

The instrument Verification Program, will be defined in compliance with the EID-A requirements and will proceed through the following phases:

- Development, aimed to demonstrate that the design, manufacturing and test process are in line with the applicable requirements (scientific goals, mission environment, spacecraft performance, spacecraft interfaces and operational requirements).

- Qualification, aimed to demonstrate that the hardware and software, produced according to the established design, is compliant to the specification requirements, including proper margins.
- Acceptance, aimed to demonstrate that the deliverable models perform in agreement with the applicable requirements and are free of workmanship defects.

The requirement verification will be performed at different levels. In particular:

- Equipment level (i.e., detectors, optics, baffles, mechanisms, electronics, software)
- Assembly level (i.e. COR, EUS, SOCS)
- System level (the whole METIS instrument)

The verification methods will be:

- Test (functional, environmental, performance tests),
- Assessment (optical, structural, thermal, electrical analysis),
- Inspection (visual determination of physical characteristics),
- Review of Design (reference to validated design documents, approved design reports, technical descriptions, engineering drawings etc., showing unambiguously that the requirements are met), or a combination thereof.

7.2 Model Philosophy

The instrument model philosophy, defined according to the satellite AIT philosophy and requirements (ref. EID-A) and to the METIS development and qualification program consists of:

- Breadboard Model (BB), already implemented during the instrument Phase B in support to the development of the METIS equipments (in particular: detectors, FEE, mechanisms, optics, baffles, electronics and software) and of the design of the thermal control and of the mechanical interfaces.
- Structural Thermal Optical Model (STOM), for the qualification by test of the METIS structure (including external occulter, baffles, optics), mechanisms, thermal control, the verification of the structural and thermal mathematical models, the verification of the instrument-S/C mechanical, thermal and optical interfaces. After the tests at instrument level, the STOM will be delivered to the Solar Orbiter Prime Contractor.
- Engineering Model (EM), for the verification of the electrical and software interfaces inside the instrument (between MPPU, FEE, detectors and mechanisms) and between the instrument and the S/C, verification of the operational modes and procedures, qualification of the instrument flight software, verification by test of the electromagnetic compatibility of the electronics, detectors and mechanisms. The MPPU and the FEE are planned to be realized at Engineering Qualification Model (EQM) level and subject to qualification tests before being used in the instrument EM. After the tests at instrument level, the STOM will be delivered to the Solar Orbiter Prime Contractor.
- Flight Model (FM), to be subjected to environmental and functional test campaign at acceptance level before the delivery the Solar Orbiter Prime Contractor.

Flight Spares (FS) for the replacement of failed or damaged equipment at integration and launch site will be also realized. The list of the items for which a FS will be realized will be defined during the instrument Phase A and discussed/agreed with ESA.

7.3 System Integration and Test Flow

Since the METIS suite is a composite instrument which includes different elements each characterized by its own specific scientific and operational task, plus some common parts, which functions are common to all the channels (MPPU, optical bench), the AIT / AIV activities at system level are of large relevance.

A diagram illustrating the flow of integration activities that shall be performed on METIS is shown in **Errore. L'origine riferimento non è stata trovata.** It includes all levels of integration from equipment (e.g. optics, detectors, mechanisms), through elements, up to system integration.

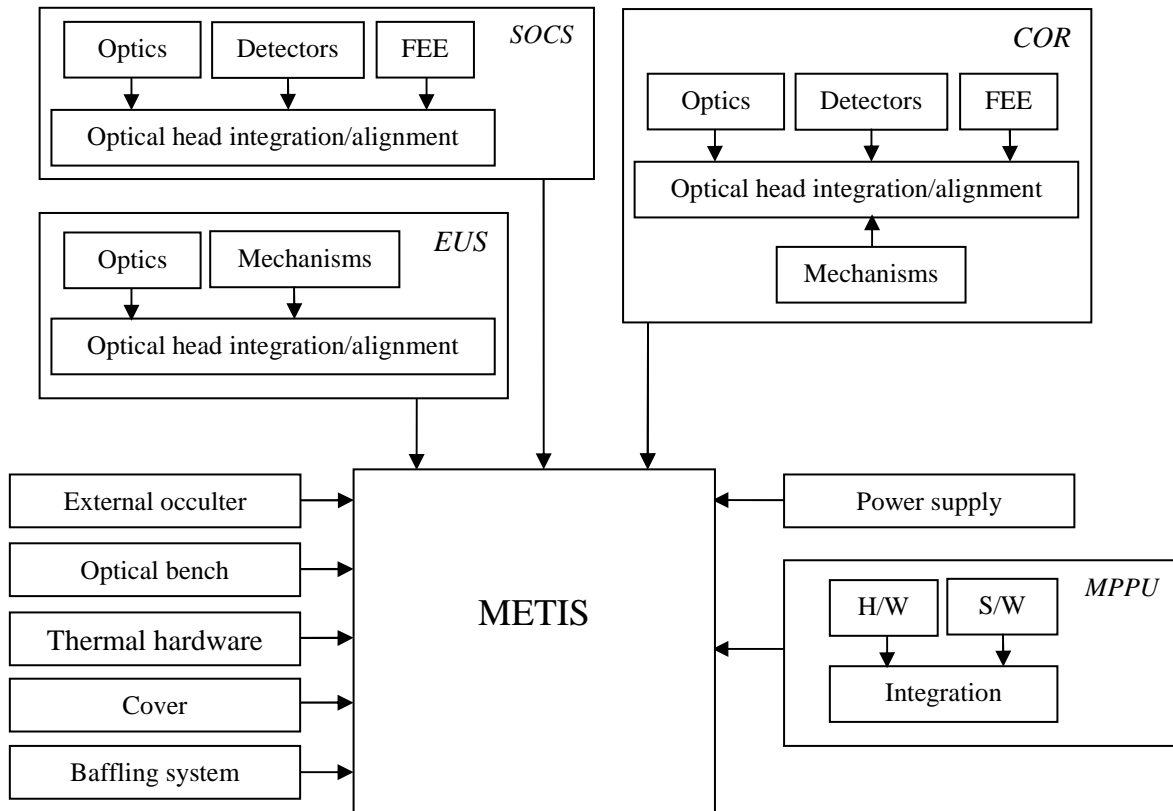


Figure 26. Flow diagram of the foreseen METIS integration activities.

7.4 Ground Support Equipment

Ground Support Equipment (GSE) is clarified in section 7.3.10 of RD1 as: “Optical, mechanical, fluidic, electrical and software support equipment or systems used for calibration, measurements, testing, simulation, transportation, handling... of space segment or of space segment elements.”

Together with each instrument model, the PI will deliver the Mechanical Ground Support Equipment (MGSE) necessary to transport, handle and integrate the instrument hardware, accompanied by appropriate documentation and proof load and calibration certificates and the Electrical Ground Support Equipment (EGSE) necessary to stimulate the instrument and to perform quick look analysis of instrument TM during system tests. The PI will remain responsible for the maintenance of this equipment and will provide the necessary manpower and expertise support to integrate the instrument EGSE into the system EGSE.

The PI will define the functional requirements of the instrument and auxiliary equipment (e.g. MGSE, EGSE, etc.) at instrument and spacecraft system level.

8 Flight Operations Concept

8.1 Observing concept

The METIS scientific observations is defined as a function of the mission phases. As baseline we adopt the orbit profile given in the Assessment Study Report, July 2000. Changes in the Solar Orbiter mission profile will reflect in the METIS Operational Concept, although maintaining the same philosophy.

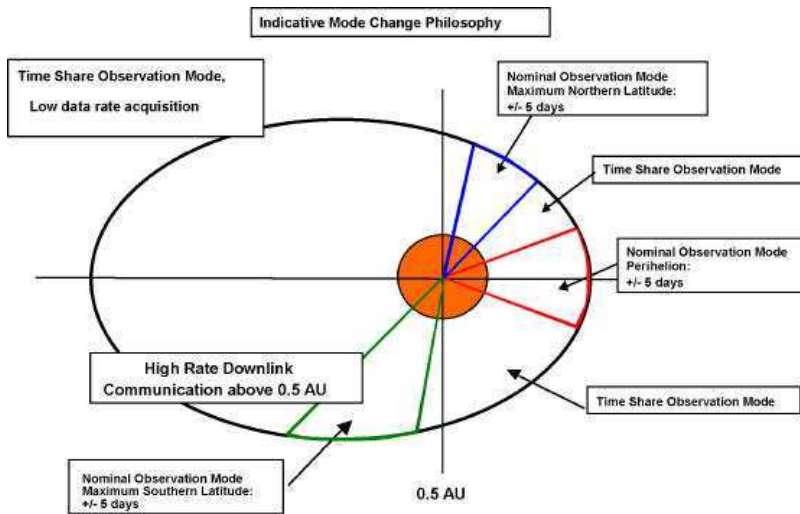


Figure 27: Modes of operation during the nominal extended mission

Nominal Observation Modes (NOM) – During the Solar Orbiter Nominal Observation Modes (3 interval, 30 days) the COR element acquires coronal Visible and UV images at high cadence (1 min) and EUV images at high cadence (2 min). Coronal images in polarized visible light and UV HI Ly α 121.6 nm are obtained for 70% and images in the EUV HeII Ly α 30.4 nm are obtained for 30% of the NOM observing time, respectively. EUS will acquire high cadence rasters (1-3 h) for 70% of the observing time. For the remaining 30% of the observing time SOCS will perform a High Cadence Sit and Stare program (1 min). SOCS and EUS are mutually exclusive from the observational point of view.

Time Share Observation Mode I (adjacent to the Nominal Observation Mode at perihelion) - In these phases, COR is obtaining coronal images at a lower cadence (10-20 min). EUS is not observing. SOCS is operating with the High Cadence Sit and Stare program.

Time Share Observation Mode II (including the aphelion) – In this phase, COR will run a low cadence (1-2 h) synoptic program, producing coronal images that will retain a space resolution better than that of LASCO C3.

According to this the data volume obtained by METIS per orbit, 29.8 GB, is compliant with the telemetry allocation foreseen for COR and EUS in the PDD. By assuming a compression factor of about 10 for the images obtained by COR and a factor of about 2 for the spectral raster and spectro-images obtained by EUS and SOCS, the required telemetry rate is 27 kb/sec.

8.2 In-Flight Calibrations

In flight calibrations will mainly consist of: a) internal calibration; b) radiometric calibration with stellar objects; c) spectral calibration with reference chromospheric lines. d) stray-light calibration during S/C nominal off-pointing.

- Radiometric calibration of EUS will be carried out by use of calibrated UV lamps installed in the METIS structure capable of illuminating the EUS telescope mirror. This type of calibration will be performed when the METIS S/C door is periodically closed.
- Observations of stellar objects will be used for in-flight calibrations of the radiometric response and the spatial resolution of COR and SOCS. The stars will be used within the nominal FOV at aphelion, and without any S/C off-pointing
- Chromospheric lines that display negligible Doppler shifts (i.e., < 1 km/s) will be used for the calibration of the spectral scale of the spectrograph for EUS and SOCS. The calibration observations will be performed at perihelion, during co-rotation, to minimize the Doppler shifts introduced by the S/C motion relative to the Sun.
- The opportunity will be seized during S/C nominal off-pointings to perform stray-light calibrations of COR and SOCS. In order to assess the instrumental stray-light behavior, disk light diffracted off the circular occulter of COR and off the linear occulter of SOCS will be allowed to enter into these two instruments in a controlled way (e.g., by fine-tuning the position of COR internal occulter). The level of stray light in SOCS will also be assessed by measuring the intensity of disk (chromospheric) lines relative to coronal lines.

8.3 Support to MOC and SOC

The total manpower dedicated to Phases 2, 3 and 4 of the programme is about 160 man-years all over the nominal duration of six years. Details are provided in the Management Plan, Part V of this proposal.

The support to MOC will be given in the pre-launch phase to set up the needed HW and perform the test procedures in preparation to instrument and scientific operations, during the commissioning phase to prepare the procedures to switch on the instrument and test its performance and during the standard operation by preparing the observation planning in

coordination with the other instruments, providing on a regular base the commands for scientific observations and calibrations, checking the instrument performances and the execution of the planned and implemented commands .

The support to SOC will be given by providing the needed HW, ensuring the data reduction and data evaluation, as soon as the telemetry data are delivered to the team, in order to check in a preliminary way the validity of the scientific data. The preliminary scientific analysis will be performed not only to trace anomalies in the expected instrumental performance but also to assess the results obtained in order to possibly optimize the scientific operations.

9 Data Reduction, Scientific Analysis And Archival Support

9.1.1 Pre-launch phase

Early in the instrument development phase, a team formed by scientists and instrument experts, from all the METIS elements, will be established to study and design all the data processing techniques that will be necessary to reformat, reduce, display and analyze the scientific data. Following this step, the second phase will consist of the development of

- 1) reformat software, to process the Level 0, raw data to the uncalibrated Level 1 data,
- 2) Data Processing and Analysis Software (DPAS), written in Interactive Data Language (IDL), to process Level 1 data to calibrated Level 2 data.

Preliminary DPAS versions will be released and used for reduction of the instrument ground calibration data. A database will be implemented to be used in the scientific data reduction process during the in-flight operations.

9.1.2 Cruise and Operation phase

A centralized METIS Operation Unit, located in one of the scientific institutions of the proposers, will be established. The METIS Operation Unit will support ESA SOC via electronic media and video-conferencing as required by the Science Management Plan, in the cruise phase and during the nominal mission. This will include the commissioning phase and the scientific operation phase.

During commissioning data reduction will be limited primarily to housekeeping data to monitor the instrument health. During the cruise phase, the first science operations with the coronagraphs will be performed and the standard data reduction will be applied.

This activity will continue during the operation phase for all the METIS elements, that is, also including EUS.

The METIS Operation Unit will process the data as soon as they will be transmitted in order to develop the necessary revisions of the data reduction procedures and to update in real time the observation catalogue. In addition the Unit will provide the data at all Levels to the Solar Orbiter ESA scientific data archive, together with observation logs and summary data.

9.1.3 Data reduction process

DPAS will be applied to the uncompressed, reformatted data to perform the standard photometric and geometric corrections, using both ground and on-board calibrations and spacecraft attitude information.

The data reduction process will result in:

Spectral Data Files: containing uncalibrated detector count data (counts per pixel) as well as instrument configuration, pointing and exposure time data. (Each observing sequence will produce one Spectral Data File per detector.)

Visible Light, UV and EUV Image Data Files: containing uncalibrated detector count data as well as instrument configuration and exposure time data, along with pointing information and information on the polarizer.

Standard Formatted Data Unit Files: will provide, for each of the above data files, a standard description

Calibration Data Files: Parameters files for pointing, spatial, wavelength and radiometric calibrations, flat field and dark count data, Solar Orbiter orbit and attitude data (TBD format).

Data Catalogs: These will include an open source database to permit users to select observations based on pointing, observation date, type of feature observed, or other criteria. They also include the Mission Log File, which records the observing sequences and other commands sent to the instrument, as well as an evaluation of the data quality. A preview of the data will allow the user to evaluate the data before the download via the data archives.

Applying the **Data Processing Analysis Software** (written in IDL, TBC) to these files the scientists are allowed to obtain calibrated data for scientific analysis.

9.1.4 Scientific data analysis

In the phase preceding launch, the scientific team will focus on the development in a coordinated fashion of all the diagnostics techniques, simulations and software codes needed for the analysis of the METIS data. This activity will run in parallel with the development of the reduction and data analysis software.

During the observation phase, the data products together with the Data Analysis Software, needed to obtain calibrated spectra and images, will be made available immediately to the METIS scientific team, and to the larger scientific community according to the ESA policy. The scientific return of the METIS investigation will be ensured and enhanced by a team policy apt, on the one hand, to address all the scientific objectives that are at the basis of the METIS proposal, and, on the other hand, promote collaboration and timely exchange of results among scientists.

Main scientific results and significant outreach material will be prepared and transmitted to ESA SOC at regular intervals.

9.1.5 Data archiving

All data categories relevant to METIS (e.g., raw, calibrated, high-level data, etc.) as well as the software libraries developed according to agreed common standards for data reduction and analysis will be transmitted to ESA SOC and most recent data will be temporarily stored in an METIS archival system compliant with the state-of-the-art data management technologies in order to provide:

- The proper data pipelining in the processing flow from the raw to the high-level stage.
- The near-real-time data ingestion and indexing (when allowed by near-real-time data availability), as requested by quick-look purposes and/or space weather applications.
- The dynamic construction of catalogs and meta-catalogs to minimize search time.
- The scheduled online delivery to the ESA Science Data Archive in the compliant format (e.g. ESA SDA and NASA NSSDC).
- The on-demand deployment of the METIS software libraries and related documentations.

Advanced capabilities like data visualization, data analysis and knowledge discovery can be implemented and added to the data products transmitted to the ESA science data archive.

9.2 Compliance with the Agency scientific data policy

METIS investigation will be fully compliant with all the requirements (as defined in the Science Management Plan) regarding scientific data policy, public relations and public outreach.

Support for Science Communication purposes will be provided to ESA.

10 Document References

10.1 Scientific Reverences

10.1.1 Chapter 2 – Scientific Objectives

- Aellig, M.R., et al., 2001, GRL, 28 (14), 2767
- Akmal, A., et al., 2001, ApJ, 553, 922
- Antiochos, S.K., 1998, ApJ, 502, L181
- Antonucci, E., et al., 1997, ApJ, 490, L183
- Antonucci, E., Abbo, L., & Doderò, M.A., 2005, A&A, 435, 699
- Antonucci, E., Abbo, L., & Telloni, D., 2006, ApJ, 643, 1239
- Aschwanden, M., et al., 2002, Sol. Phys. 206, 99
- Bemporad, A., et al., 2006, ApJ, 638, 1110
- Bemporad, A., et al., 2007, ApJ, 655, 576
- Ciaravella, A., et al., 1997, ApJ, 491, L59
- Ciaravella, A., et al., 2002, ApJ, 575, 1116
- Ciaravella, A., Raymond, J. C., Kahler, et al. 2005, ApJ, 621, 1121
- Cranmer, S.R., 2002, Space Sci. Rev., 101, 229
- De Pontieu, B., et al., 2007, Science. 318, 1574
- Einaudi, G., et al. 1999, JGR, 104, 521
- Fisk, L.A., et al. 1999, ApJ, 521, 868
- Fisk, L.A., & Schwadron, N.A., 2001, ApJ, 560, 425
- Forbes, T.G., & Isenberg, P.A., 1991, ApJ, 373, 294
- Gabriel, A.H., et al., 2003, ApJ, 589, 623
- Galsgaard K., et al., 2007, ApJ, 666, 516
- Geiss, J., et al., 1970, Sol. Phys., 12, 458
- Giordano, S., et al., 2000, ApJ, 531, L79
- Gopalswamy, N., et al., 2001, JGR, 106, 25261
- Gopalswamy, N., et al., 2003, ApJ, 586, 562
- Gopalswamy, N., et al., 2004, JGR, 109, A12105
- Hassler, D., et al., 1999, Science, 283
- Innes, D.E., et al., 1997, Nature, 386, 811
- Harrison, R.A., 1997, Sol. Phys., 175, 467
- Klimchuk, J. A., 2006, Sol. Phys., 234, 41
- Laming, J.M., 2004, ApJ, 614, 1063,
- Lopez Fuentes, M.C., Klimchuk, J. A, & Demoulin, P., 2006, ApJ, 639, 459
- Low, B.C., 1996, in: ASP Conf. Series, 95, 148
- Mancuso, S. 2007, A&A, 463, 1137
- Mancuso, S., Raymond, J. C., Kohl, J., et al. 2002, A&A, 383, 267
- Mancuso, S., Raymond, J. C., Kohl, J., et al. 2003, A&A, 400, 347
- Mancuso, S., & Raymond, J. C. 2004, A&A, 413, 363
- Mann, G., et al., 2003, A&A, 400, 329
- Marocchi, D., et al., 2001, Annal. Geophys., 19, 135
- Neugebauer, M., et al., 2002, JGR, 107, 306
- Noci, G., et al. 1997, in The Corona and Solar Wind near Minimum Activity, ed.O.Kjeldseth-Moe (Noordwijk: ESA SP-404), 75
- Noci, G. & Gavryuseva, E., 2007, ApJ, 658, L63
- Rakowski, C.E., et al., 2007, ApJ, 667, 602, 2007
- Raymond, J.C., et al., 1997, Sol. Phys., 175, 645
- Raymond, J. C., et al. 2000, Geoph. Res. Lett. 27, 1439
- Raymond, J.C., et al., 2003, ApJ, 597, 1106

- Reale, F., et al., 2007, *Science*, 318, 1582
- Reames, D. V., Kahler, S. W., & Ng, C. K. 1997, *ApJ*, 491, 414
- Schwadron, N.A., et al. 1999, *ApJ*, 521, 859
- Spadaro, D., Zuccarello, F., & Zappala, R. A., 1996, *A&A*, 308, 970
- Strachan, L., Suleiman, R., Panasyuk, A.V., Biesecker, D.A., & Kohl, J.L., 2002, *ApJ*, 571, 1008
- Telloni, D., Antonucci, E., & Doderò, M.A., 2007, *A&A*, 472, 299
- Teriaca, L., Poletto, G., Romoli, M., & Biesecker, D.A., 2003, *ApJ*, 588, 566
- Tu, C.-Y., et al., 2005, *Science*, 308, 519
- Ventura, et al., 2002, *A&A*, 395, 975
- Verdini, A., & Velli, M., 2007, *ApJ*, 662, 669
- Wang, Y.-M., et al. 2000, *JGR*, 105, 25133
- Wang, Y.-M., & Sheeley, N.R., 1990, *ApJ*, 355, 726
- Wiegmann, T., et al. 2000, *Sol. Phys.*, 191(2), 391

10.1.2 Chapter 3 - Instrument Performances

- Andretta, V., Mauas, P. J. D., Falchi, A., & Teriaca, L. (2007), submitted to *ApJ*
- Landi, E., Del Zanna, G., Young, P. R., Dere, K. P., Mason, H. E., & Landini, M. (2006), *ApJS*, **162**, 261-280
- Feldman, U.; Landi, E., Laming, J. M. (2005), *ApJ*, 619, 1142-1152
- Laming, J. M.; Feldman, U. (2003), *ApJ*, 591, 1257-1266
- Laming, J. M.; Feldman, U. (2001), *ApJ*, 546, 552-558
- Landi, E., Del Zanna, G., Young, P. R., Dere, K. P., Mason, H. E., & Landini, M. (2006), *ApJS*, 162, 261-280
- Vernazza, J. E., & Reeves, E. M. (1978), *ApJS*, **37**, 485-513
- Warren, H. P., Mariska, J. T., Wilhelm, K. (1998), *ApJS*, **119**, 105-120
- Wilhelm, K., et al. (1998), *A&A*, **334**, 685-702

10.1.3 Chapter 4 - Instrument Technical Description and Design

- S. Fineschi, C. M. Korendyke, J. D. Moses, and R.J. Thomas, "Solar ultraviolet spectro-coronagraph with toroidal varied line-space (TVLS) grating", *Proc. SPIE* **5487**, 1165 (2004)
- S. Fineschi, J.D. Moses, and R.J. Thomas, "Spectro-imaging of the extreme-UV solar corona" *Proc. SPIE* **5901**, 289 (2005)
- D.L. Windt, S. Donguy, J. Seely, and B. Kjørntrattanawanich, "Experimental comparison of extreme-ultraviolet multilayers for solar physics", *Appl. Opt.* **43**, 1835 (2004)
- M.-G. Pelizzo, D. Gardiol, P. Nicolosi, A. Patelli, and V. Rigato, "Design, deposition, and characterization of multilayer coatings for the Ultraviolet and Visible-Light Coronagraphic Imager", *Appl. Opt.* **43**, 2661 (2004)
- H. Takenaka, S. Ichimaru, T. Ohchi, and E.M. Gullikson, "Soft-X-ray reflectivity and heat resistance of SiC/Mg multilayer", *Jnl. Electr. Spectr. Rel. Phen.* **144**, 1047 (2005)
- J.L. Kohl et al, "Ultraviolet Coronagraph Spectrometer for the Solar and Heliospheric Observatory", *Sol. Phys.* **162**, 313 (1995)
- Naletto, G., et al, *Appl. Opt.* 44, 5046 (2005)
- Landini, F., et al, *Appl. Opt.* 45, 6657 (2006)
- Romoli, M. et al., (2007) ESA SP-641
- Fineschi, S., et al, *Proc. SPIE* 5901 (2005)
- Thomas, R.J. (2002), *Proc. SPIE* 4853, 411
- L. Poletto, R.J. Thomas (2004), *Appl. Opt.* 43, 2029
- Harvey, J.E., Vernold, C.L. (1997), *Proc. SPIE* 3141, 113
- Teriaca, L., et al, D.A. (2003) *ApJ* 566, 588
- Larruquert, J.I., Keski-Kuha, R.A.M. (2000), *Appl. Opt.* 39, 1537
- Kortright, J.B., Windt, D.L. (1988) *Appl. Opt.* 27, 2841
- Blumenstock, G.M., Keski-Kuha, R.A.M. (1994), *Appl. Opt.* 33, 5962
- Keski-Kuha, et al (1998) *Appl. Opt.* 37, 8038

- Siegmund, O.W, et al (1987), Appl. Opt. 26, 3607
- Larruquert, J.I., (2002) Appl. Opt. 41, 2532
- Wilhelm, K. et al (1995), Sol. Phys. 162, 189
- Uslenghi, M. et al, Proc. SPIE 4498 (2001)
- Bonanno, G. et al, Proc. SPIE 4498 (2001)
- Tremsin, A.S., Siegmund, O.H.W., Proc. SPIE 5920 (2005)
- Schühle, U. et al (2007) ESA SP-641
- Fineschi, S., et al (2004), Proc. SPIE 5487, 1165 (2004)
- Fineschi, S., Moses, J.D., R.J. Thomas (2005), Proc. SPIE 5901, 289
- Windt, D.L., et al (2004) Appl. Opt. 43, 1835
- Pelizzo, M.-G., et al (2004) Appl. Opt. 43, 2661
- Takenaka, H., et al (2005), Jnl. Electr. Spectr. Rel. Phen. 144, 1047
- Kohl, J.L. et al (1995), Sol. Phys. 162, 313

11 Acronyms

ADC	Analog to Digital Converter
AFT	Abbreviated Functional Test
AIT	Assembly, Integration and Test
AOCS	Attitude and Orbit Control System
APS	Active Pixel Sensor
BB	Breadboard
BBM	Bread-Board Model
CCD	Charge Couple Device
CFRP	Carbon Fiber Reinforced Plastic
CME	Coronal Mass Ejections
CNR	Consiglio Nazionale delle Ricerche
CNRS	Centre National de la Recherche Scientifique
CoI	Co-Investigator
CoM	Center of Mass
CoPI	Co-Principal Investigator
COR	METIS Visible and EUV Coronagraphic imager
CTE	Coefficient of Thermal Expansion
DMS	Data Management System
ECSS	European Cooperation for Space Standardization
EEO	Extended External Occulter
EEOM	EEO Mechanism
EM	Electrical Model
EM	Experiment Manager
EO	External occulter
EOM	External occulter Mechanism
EQM	Electrical Qualification Model
ESA	European Space Agency
EUI	EUV Imager
EUS	METIS EUV disk Spectrometer
EUV	Extreme UltraViolet
EUVC	EUV Channel
FEE	Front End Electronics
FEM	Filter Exchange Mechanism
FFT	Full Functional Test
FM	Flight Model
FOV	Field Of View
FS	Flight Spare
FWHM	Full Width at Half Maximum
GSE	Ground Support Equipment
H/W	Hardware
HeF	Aluminum low-pass filter of the coronagraph
HELEX	Heliophysical Explorers
HERSCHEL	Helium Resonance Scattering in the Corona and Heliosphere
HF	Narrow-band multilayer filter of the coronagraph
HGA	High Gain Antenna
HVPS	High Voltage Power Supply
HWRP	Half Wave Retarder Plate
IAC	Instituto de Astrofísica de Canarias
IAPS	Intensified APS
IAS	Institut d'Astrophysique Spatiale
IASF	Istituto di Astrofisica Spaziale e Fisica cosmica
IDP	Instrument Development Plan
IFE	Instrument Front End
IFSI	Istituto di Fisica dello Spazio Interplanetario



ILS	Instrument Line of Sight
INAF	Istituto Nazionale di AstroFisica
INFM	Istituto Nazionale Fisica della Materia
IO	Internal Occulter
IOM	Internal Occulter Mechanism
IR	Infrared
LAM	Laboratoire d'Astrophysique de Marseille
LCL	Latching Current Limiters
LCVR	Liquid Crystal Variable Retarder
M0	Sun-disk rejection mirror of the coronagraph
M1	Primary mirror of the coronagraph
M2	Secondary mirror of the coronagraph
MCP	Micro Channel Plate
METIS	Multi Element Telescope for Imaging and Spectroscopy
MGSE	Mechanical Ground Support Equipment
ML	Multilayer
MOC	Mission Operation Center
Mol	Moment of Inertia
MPPU	METIS Processing & Power Unit
MPS	Max-Planck-Institut fuer Sonnensystemforschung
MSSL	Mullard Space Science Laboratory
N/A	Not Applicable
NASA	National Aeronautics and Space Administration
NOM	Nominal Observing Mode
NRL	Naval Research Laboratory
OAA	Osservatorio Astronomico di Arcetri
OACN	Osservatorio Astronomico di Capodimonte Napoli
OACt	Osservatorio Astronomico di Catania
OAPa	Osservatorio Astronomico di Palermo
OAR	Osservatorio Astronomico di Roma
OATo	Osservatorio Astronomico di Torino
OATs	Osservatorio Astronomico di Trieste
OGSE	Optical Ground Support Equipment
OP	Off Pointing
PA	Product Assurance
PI	Principal Investigator
PoliTo	Politecnico di Torino
QE	Quantum Efficiency
RD-n	Reference Document n
S/C	Spacecraft
S/W	Software
SC	Sun Center
SCORE	Sounding-rocket Coronagraphic Experiment
SEP	Solar Energetic Particles
SMM	Structural Mathematical Model
SO	Solar Orbiter
SOCS	METIS Solar Orbiter Coronal Spectrometer
SOHO	Solar and Heliospheric Observatory
STOM	Structural Thermal Optical Model
TBC	To Be Confirmed
TBD	To Be Defined
TBW	To Be Written
TEC	Thermo Electric Cooler
TM	Telemetry
TSOM	Time Share Observing Mode
TVLS	Toroidal Variable Line Space
UFOV	Unobstructed Field Of View

UniAq	Università di Aquila
UniCal	Università della Calabria
UniFi	Università di Firenze
UniPD	Università di Padova
UniPd	Università di Padova
UniPg	Università di Perugia
UniPv	Università di Pavia
UniRm	Università di Roma
UORF	Unit Optical Reference Frame
URF	Unit Reference Frame
UV	Ultraviolet
UVC	UV channel
UVD	Ultraviolet Detector
VD	Visible Detector
VIM	Visible Imager & Magnetograph
VLC	Visible Light Channel
VUV	Vacuum ultraviolet